

Elastic Scattering and Transport Coefficients for a Quark Plasma in $SU_f(3)$ at Finite Temperatures

P. Rehberg*, S. P. Klevansky and J. Hüfner

Institut für Theoretische Physik, Universität Heidelberg,

Philosophenweg 19, D-69120 Heidelberg, Germany

(April 1996)

Abstract

The temperature dependence of the elastic scattering processes $qq' \rightarrow qq'$ and $q\bar{q}' \rightarrow q\bar{q}'$, with $q, q' = u, d, s$ is studied as a function of the scattering angle and the center of mass energy of the collision within the framework of the $SU_f(3)$ Nambu–Jona–Lasinio model. Critical scattering at threshold is observed in the $q\bar{q}' \rightarrow q\bar{q}'$ process, leading to an enhancement of the cross section as occurs in the phenomenon of critical opalescence. Transport properties such as viscosity, mean free paths and thermal relaxation times are calculated. Strangeness enhancement is investigated via the chemical relaxation times, which are found to be considerably higher than those calculated via perturbative QCD. A comparison with the experimental values for the strangeness enhancement in $S + S$ collisions leads to an upper limit of 4 fm/c for the lifetime of the plasma.

PACS numbers: 11.30.Rd, 12.38.Mh, 24.85.+p, 11.10.Wx

*E-Mail: Peter@Frodo.TPhys.Uni-Heidelberg.DE

I. INTRODUCTION

With the proposed experiments for heavy ion collisions at the LHC coming closer, the onus has settled on the theoretical physics community to provide a clear, coherent and credible description of such collisions. One of the major goals, that of detecting the presence of plasma formation of the constituent quarks and gluons is for both theorists and experimentalists alike, a formidable task. Such a phase is believed to be formed as matter is deconfined.

From the theoretical side, a description that goes beyond the standard equilibrium statistical approaches is necessitated by the short collision time of the ions, since this may preclude equilibration of all degrees of freedom. Thus a transport theory that is consistently based on quantum chromodynamics (QCD) itself is required. While such formulations have been set up by some authors [1,2], they have not reached the stage where they can be implemented to provide original physical results.

One step in this direction is to examine the consequences of a transport theory based on an effective model of QCD, that exhibits some important features of the theory. In particular, it is desirable to see if any major effects due to the exhibited feature are observable in the final analysis.

It is well-known that the low energy particle sector is well described by effective chiral theories of QCD. We therefore choose to implement the Nambu–Jona-Lasinio (NJL) model [3–5] in its three flavor extension for such a study. This model has the advantage that, being a model, it can be studied over the entire temperature range. The NJL model also offers a simple intuitive view of chiral symmetry breakdown and restoration via a realization of the pairing mechanism of quark and antiquark states of an effective interaction in a similar sense to the BCS theory of superconductivity. The model suffers however from several unaesthetic diseases: the simple form of a point-like interaction, while making the model analytically tractable, also ensures its nonrenormalizability, and a cutoff scale Λ for the theory must be introduced. A confinement / deconfinement phase transition cannot occur. Rather a “soft” form of deconfinement is observed at the so-called Mott temperature, at which the mesons dissociate into their constituents [6].

The NJL model, being a strong coupling field theory, cannot be handled in

perturbation theory. The by now standard technique is a self-consistent expansion of quantities to be calculated in the inverse number of colors $1/N_c$ [7]. It is this expansion, taken to lowest order, that we use in our model.

In order to make some progress in the ambitious task presented, we have already studied hadronization processes of quarks and antiquarks into two mesons, $q\bar{q}' \rightarrow MM'$ [8], within the $SU_f(3)$ NJL model. In addition, we require the elastic scattering cross sections for both quarks and quarks $qq' \rightarrow qq'$ and quarks and antiquarks $q\bar{q}' \rightarrow q\bar{q}'$ within the three flavor model. The cross sections for the third possible class, $\bar{q}\bar{q}' \rightarrow \bar{q}\bar{q}'$, follow immediately from $q\bar{q}' \rightarrow q\bar{q}'$ by time reversal invariance, as long as no chemical potential is involved. It is the purpose of this paper to calculate these cross sections, together with the attendant transport properties (mean free paths and shear viscosities) in the $SU_f(3)$ model for realistic values of the current quark masses $m_{0u} = m_{0d} = 5.5$ MeV, $m_{0s} = 140$ MeV. We note that some elastic scattering cross sections have been calculated in the two flavor sector with the additional restriction of the chiral limit condition $m_{0u} = m_{0d} = 0$ in Ref. [9]. As will be seen, the extension presented here indicates significant increases in the cross sections due to additional available channels.

The quark quark scattering cross sections are relatively featureless. On the other hand, quark antiquark scattering shows a threshold divergence at the Mott temperature $T_{M\pi}$, at which the pion dissociates into its constituents. At higher temperatures that are to be expected in the plasma phase, a large resonant structure is observed, that is a remnant of this feature of critical scattering. This is however not directly observable. When these cross sections are included in a fully consistent transport theory based on this chiral model of QCD, it is hoped that this may lead to observable effects.

We have also studied transport coefficients within this model. We find that the viscosity coefficient η/T^3 lies in the range 0.83 to 1.0 per flavor degree of freedom for light quarks, and is slightly lower for strange quarks, being 0.68 to 0.75, i.e. the *total* viscosity is found to lie between 3.2 and 4.0 considering only two flavors, while for three flavors the total viscosity would lie between 4.6 and 5.5. Perturbative QCD estimates lie slightly higher than this value: a variational calculation [10] (see also [11]) gives $\eta/T^3 \approx -1.16/(\alpha_s^2 \log \alpha_s)$ for two quark flavors, where α_s is the strong coupling strength. One finds the value $\eta/T^3 \approx 6.3$ at $\alpha_s = 0.6$. This should

be viewed somewhat critically, since this perturbative formula is strictly valid for $\alpha_s \ll 1$, and is an extremely sensitive function of α_s . In the strongly interacting non-perturbative regime, it is not applicable. Hydrodynamical estimates, on the other hand [12], give a wide range for this quantity, $2 < \eta/T^3 < 3\tau T$, where τ is the proper time for the expansion of the system. We also calculate mean free paths for light and heavy flavors and these are found to be of the order of magnitude of 1 fm. The thermal relaxation times are found to vary between 1–2 fm/ c , with that of the strange quark being slightly higher.

In order to discuss strangeness enhancement, we examine the chemical relaxation time for strange quarks within the model. These, lying between 11 fm/ c and 17 fm/ c , are considerably higher than the naive perturbative QCD prediction of Ref. [13] that proceeds via gluon fusion. The origin of this discrepancy can be traced back to the value of the strange quark mass m_s . In the perturbative QCD calculation of Ref. [13], the physical mass was assumed to be equal to the current quark mass value. In the NJL model, on the other hand, a significantly enhanced value of the strange quark mass is still found at temperatures of the order of 250 MeV [8]. In fact it is at least twice the current quark mass value. A recalculation of the perturbative QCD calculation using the temperature dependent NJL masses gives relaxation times of the same order of magnitude as our calculation. We note that an assessment of the relevance of quark antiquark scattering for the strangeness enhancement that is observed e.g. in $S + S$ collisions, depends on the plasma lifetime. Our calculations would attribute the observed enhancement to these processes for a plasma lifetime of ca. 4 fm/ c . Such a value is supported by hydrodynamical calculations [14–16]. This places an upper limit on the plasma lifetime. For shorter times, other mechanisms, including hadronization [8] and final state interactions must also be invoked.

Our paper is organized as follows: In Section II, we first give a brief review of essential formalism, then we discuss quark quark scattering in the nonstrange and strange sectors. Following this, quark antiquark scattering for both nonstrange and strange partons is presented. Transport properties are derived and discussed in Section III. The possibility of strangeness enhancement due to quark antiquark scattering is discussed in Section IV. A general discussion of our methods and results is presented in Section V. We summarize and conclude in Section VI.

II. SCATTERING PROCESSES

A. Review of Formalism

The model which we employ for our calculations is the $SU_f(3)$ version of the Nambu–Jona–Lasinio (NJL) model [4,5] considered at finite temperature. In this subsection, we give a brief review of the basic formalism and define our notation, without giving derivations of our formulae. For a more detailed treatment, the reader is referred to Refs. [4,5,8,17]. The Lagrangian for this model is

$$\begin{aligned} \mathcal{L} = & \sum_{f=u,d,s} \bar{\psi}_f (i\cancel{\partial} - m_{0f}) \psi_f + G \sum_{a=0}^8 \left[(\bar{\psi} \lambda^a \psi)^2 + (\bar{\psi} i \gamma_5 \lambda^a \psi)^2 \right] \\ & - K \left[\det \bar{\psi} (1 + \gamma_5) \psi + \det \bar{\psi} (1 - \gamma_5) \psi \right] , \end{aligned} \quad (2.1)$$

where G and K are coupling constants with dimensions $[\text{MeV}]^{-2}$ and $[\text{MeV}]^{-5}$ respectively, and m_{0f} are the current masses for quarks of flavor f , which explicitly break chiral symmetry. The determinantal term leads to the appearance of six fermion vertices, which, in a mean field approximation, can be reduced to an effective four point interaction by contracting out $\bar{\psi}\psi$ pairs [4]. Under the additional assumption of $SU_f(2)$ isospin symmetry, $m_u = m_d$, this leads to the effective Lagrangian

$$\begin{aligned} \mathcal{L} = & \sum_{f=u,d,s} \bar{\psi}_f (i\cancel{\partial} - m_{0f}) \psi_f + \sum_{a=0}^8 \left[K_a^- (\bar{\psi} \lambda^a \psi)^2 + K_a^+ (\bar{\psi} i \gamma_5 \lambda^a \psi)^2 \right] \\ & + K_{08}^- \left[(\bar{\psi} \lambda^8 \psi)(\bar{\psi} \lambda^0 \psi) + (\bar{\psi} \lambda^0 \psi)(\bar{\psi} \lambda^8 \psi) \right] \\ & + K_{08}^+ \left[(\bar{\psi} i \gamma_5 \lambda^8 \psi)(\bar{\psi} i \gamma_5 \lambda^0 \psi) + (\bar{\psi} i \gamma_5 \lambda^0 \psi)(\bar{\psi} i \gamma_5 \lambda^8 \psi) \right] \end{aligned} \quad (2.2)$$

with the effective coupling constants

$$\begin{aligned} K_0^\pm &= G \mp \frac{1}{3} K (2\mathcal{G}^u + \mathcal{G}^s) , & K_1^\pm &= K_2^\pm = K_3^\pm = G \pm \frac{1}{2} K \mathcal{G}^s , \\ K_4^\pm &= K_5^\pm = K_6^\pm = K_7^\pm = G \pm \frac{1}{2} K \mathcal{G}^u , & K_8^\pm &= G \pm \frac{1}{6} K (4\mathcal{G}^u - \mathcal{G}^s) , \\ K_{08}^\pm &= \pm \frac{\sqrt{2}}{6} K (\mathcal{G}^u - \mathcal{G}^s) , \end{aligned} \quad (2.3)$$

expressed in terms of the couplings G , K , and the trace of the Green function $S_f(x, x)$ via

$$\mathcal{G}^f = N_c \text{itr}_\gamma S_f(x, x) = -\frac{N_c}{4\pi^2} m_f A(m_f, \mu_f) , \quad (2.4)$$

where, in the case of finite temperature and chemical potential,

$$A(m_f, \mu_f) = \frac{16\pi^2}{\beta} \sum_n e^{i\omega_n \eta} \int_{|\vec{p}| < \Lambda} \frac{d^3 p}{(2\pi)^3} \frac{1}{(i\omega_n + \mu_f)^2 - (\vec{p}^2 + m_f^2)} \quad . \quad (2.5)$$

In this expression, ω_n are the Matsubara frequencies for fermions, $\omega_n = (2n+1)\pi/\beta$, and the sum runs over all positive and negative integer values. Note that this quantity is derived from the finite temperature Green function

$$S_f(\vec{x} - \vec{x}', \tau - \tau') = \frac{i}{\beta} \sum_n e^{-i\omega_n(\tau - \tau')} \int \frac{d^3 p}{(2\pi)^3} \frac{e^{i\vec{p}(\vec{x} - \vec{x}')}}{\gamma_0(i\omega_n + \mu_f) - \vec{\gamma}\vec{p} - m_f} \quad . \quad (2.6)$$

Explicit expressions for $A(m, \mu)$, which are suitable for numerical evaluation, can be found in Ref. [17]. Note that we employ a three momentum cutoff Λ in order to make the integral in Eq. (2.5) finite. The physical quark masses m_u , m_d , m_s are calculated from the three coupled gap equations

$$m_i = m_{0i} - \frac{GN_c}{\pi^2} m_i A(m_i, \mu_i) + \frac{KN_c^2}{8\pi^4} m_j A(m_j, \mu_j) m_k A(m_k, \mu_k) \quad , \quad (2.7)$$

where i, j, k are three pairwise distinct flavors. An explicit numerical solution of Eq. (2.7) can be found in Ref. [8].

Mesons are constructed by calculating the quark–antiquark effective interaction within the random phase approximation [4,5]. In the pseudoscalar sector, this leads to the explicit form for the pion and kaon propagators

$$\mathcal{D}_\pi(p_0, \vec{p}) = \frac{2K_3^+}{1 - 4K_3^+ \Pi_{u\bar{u}}^P(p_0, \vec{p})} \quad (2.8)$$

$$\mathcal{D}_K(p_0, \vec{p}) = \frac{2K_4^+}{1 - 4K_4^+ \Pi_{u\bar{s}}^P(p_0, \vec{p})} \quad . \quad (2.9)$$

The irreducible pseudoscalar polarization function $\Pi_{f\bar{f}'}^P$, required in Eqs. (2.8) and (2.9) is given explicitly by [8]

$$\begin{aligned} \Pi_{f\bar{f}'}^P(p_0, \vec{p}) = & -\frac{N_c}{8\pi^2} \left\{ A(m_f, \mu_f) + A(m_{f'}, \mu_{f'}) \right. \\ & \left. + \left[(m_f - m_{f'})^2 - (p_0 + \mu_f - \mu_{f'})^2 + \vec{p}^2 \right] B_0(\vec{p}, m_f, \mu_f, m_{f'}, \mu_{f'}, p_0) \right\} \quad , \end{aligned} \quad (2.10)$$

where B_0 is the analytical continuation of

$$B_0(\vec{p}, m_f, \mu_f, m_{f'}, \mu_{f'}, i\nu_m) = \frac{16\pi^2}{\beta} \sum_n e^{i\omega_n \eta} \int_{|\vec{q}| < \Lambda} \frac{d^3q}{(2\pi)^3} \frac{1}{[(i\omega_n + \mu_f)^2 - E_f^2]} \frac{1}{[(i\omega_n - i\nu_m + \mu_{f'})^2 - E_{f'}^2]} \quad (2.11)$$

($E_f = \sqrt{\vec{q}^2 + m_f^2}$, $E_{f'} = \sqrt{(\vec{q} - \vec{p})^2 + m_{f'}^2}$) to the real axis. Explicit expressions for B_0 can again be found in [17].

For the η and η' , the situation is somewhat more involved due to the mixing terms in Eq. (2.2). The quark–antiquark scattering matrix containing these particles is a 2×2 matrix

$$\mathcal{D}_{\eta, \eta'} = 2 \frac{\mathcal{K}}{\mathcal{A}\mathcal{C} - \mathcal{B}^2} \begin{pmatrix} \mathcal{A} & \mathcal{B} \\ \mathcal{B} & \mathcal{C} \end{pmatrix} \quad (2.12)$$

with

$$\mathcal{A} = K_0^+ - \frac{4}{3} \mathcal{K} (\Pi_{u\bar{u}}^P + 2\Pi_{s\bar{s}}^P) \quad (2.13a)$$

$$\mathcal{B} = K_{08}^+ + \frac{4\sqrt{2}}{3} \mathcal{K} (\Pi_{u\bar{u}}^P - \Pi_{s\bar{s}}^P) \quad (2.13b)$$

$$\mathcal{C} = K_8^+ - \frac{4}{3} \mathcal{K} (2\Pi_{u\bar{u}}^P + \Pi_{s\bar{s}}^P) \quad (2.13c)$$

$$\mathcal{K} = K_0^+ K_8^+ - K_{08}^2 \quad . \quad (2.13d)$$

Since we do not require the meson masses and their static properties explicitly in this work, we do not display the technical details needed for this here, but rather refer our reader to Ref. [8].

In the scalar sector, the NJL model in its $SU_f(3)$ version contains nine mesons (σ_{π^0} , σ_{π^\pm} , σ_{K^0} , $\sigma_{\overline{K^0}}$, σ_{K^\pm} , σ , σ'), that accompany the nine mesons (π^0 , π^\pm , K^0 , $\overline{K^0}$, K^\pm , η , η') in the pseudoscalar sector. The propagators for the scalar particles can be immediately obtained from Eqs. (2.8)–(2.13) by replacing the pseudoscalar coupling strengths K_i^+ by the scalar ones K_i^- and replacing the pseudoscalar polarization by the scalar polarization

$$\Pi_{f\bar{f}'}^S(p_0, \vec{p}) = -\frac{N_c}{8\pi^2} \left\{ A(m_f, \mu_f) + A(m_{f'}, \mu_{f'}) + \left[(m_f + m_{f'})^2 - (p_0 + \mu_f - \mu_{f'})^2 + \vec{p}^2 \right] B_0(\vec{p}, m_f, \mu_f, m_{f'}, \mu_{f'}, p_0) \right\} \quad (2.14)$$

Via Eqs. (2.8), (2.9) and (2.12), the masses of the pseudoscalar mesons as well as those of the scalar mesons with the appropriate changes mentioned above, have been obtained as a function of temperature. For explicit values see Ref. [8].

B. Quark Quark Scattering

In this subsection, we classify and illustrate via calculation the possible independent elastic scattering collision processes within the $SU_f(3)$ flavor quark–quark combinations.

For elastic scattering processes of the type $qq' \rightarrow qq'$, via simple combinatorics we have six different possibilities available. However, due to isospin symmetry, the processes $us \rightarrow us$ and $ds \rightarrow ds$ lead to the same cross section. The same holds true for the processes $uu \rightarrow uu$ and $dd \rightarrow dd$, so that we have in total only four independent processes for quark–quark scattering. These are listed in Table I. The Feynman diagrams appropriate for such scattering in lowest order in terms of a $1/N_c$ expansion, where N_c is the number of colors, are shown in Fig. 1. Here both t –channel and u –channel diagrams can occur, with the species of the exchanged meson depending on the specific process in question. These are also given explicitly in Table I for each of the independent processes. We note that there is *at least* one scalar and one pseudoscalar exchange channel for each diagram. In this point, this $SU_f(3)$ chiral model differs markedly from the $SU_f(2)$ chiral model, as is evident from the fact that the $SU_f(2)$ model supports only one scalar meson. This will be seen explicitly in the numerical calculations.

In the following, we will derive as far as possible general expressions for the cross sections. We illustrate these with explicit calculations for the specific process $uu \rightarrow uu$.

1. Analytical Calculations

The matrix elements corresponding to the Feynman graphs of Fig. 1 can in general be written as

$$\begin{aligned}
 -i\mathcal{M}_t &= \delta_{c_1,c_3}\delta_{c_2,c_4}\bar{u}(p_3)Tu(p_1)\left[i\mathcal{D}_t^S(p_1-p_3)\right]\bar{u}(p_4)Tu(p_2) \\
 &\quad + \delta_{c_1,c_3}\delta_{c_2,c_4}\bar{u}(p_3)(i\gamma_5 T)u(p_1)\left[i\mathcal{D}_t^P(p_1-p_3)\right]\bar{u}(p_4)(i\gamma_5 T)u(p_2) \quad (2.15)
 \end{aligned}$$

$$\begin{aligned}
 -i\mathcal{M}_u &= \delta_{c_1,c_4}\delta_{c_2,c_3}\bar{u}(p_4)Tu(p_1)\left[i\mathcal{D}_u^S(p_1-p_4)\right]\bar{u}(p_3)Tu(p_2) \\
 &\quad + \delta_{c_1,c_4}\delta_{c_2,c_3}\bar{u}(p_4)(i\gamma_5 T)u(p_1)\left[i\mathcal{D}_u^P(p_1-p_4)\right]\bar{u}(p_3)(i\gamma_5 T)u(p_2) \quad . \quad (2.16)
 \end{aligned}$$

Here $T\mathcal{D}_t^S T$ is a symbolic expression for the sum over all scalar t exchange channels of flavor factors times particle propagator, with $T\mathcal{D}_t^P T$ being the same for pseudoscalar t graphs. The symbols $T\mathcal{D}_u^S T$ and $T\mathcal{D}_u^P T$ are the analogous quantities for the u -channel. Note that the matrix elements (2.15) and (2.16) describe the scattering due to the exchange of colorless mesons. The scattering cross sections due to the exchange of color octet states can be estimated to differ from Eqs. (2.15), (2.16) by a factor 4/9 [9] and are neglected here.

To calculate the cross sections, we require the squared matrix elements, summed over spin and color degrees of freedom and averaged over the incoming states,

$$\frac{1}{4N_c^2} \sum_{s,c} |\mathcal{M}_t - \mathcal{M}_u|^2 \quad . \quad (2.17)$$

General expressions for these, apart from the flavor factors stemming from the Gell-Mann matrices, are given in Appendix A. The flavor factors, together with the propagators of the exchanged mesons, have to be specified for each individual process. We illustrate this procedure explicitly here for the process $uu \rightarrow uu$. From Table I, we read off that the t -channel exchange proceeds via an π^0 , η and η' in the pseudoscalar sector and via a σ_{π^0} , σ and σ' in the scalar sector. This means that the propagators for the t -channel have the form

$$T\mathcal{D}_t^P T = \mathcal{D}_\pi + \frac{4}{3} \frac{\mathcal{K}}{\mathcal{A}\mathcal{C} - \mathcal{B}^2} \left(\mathcal{A} + \sqrt{2}\mathcal{B} + \frac{1}{2}\mathcal{C} \right) \quad , \quad (2.18)$$

where \mathcal{D}_π is defined in Eq. (2.8) and \mathcal{A} , \mathcal{B} , \mathcal{C} and \mathcal{K} are given by Eq. (2.13). The propagator for the scalar t -channel has the same form with, however, the coupling constants and polarization functions suitably altered, as was discussed in Sec. II A. The u -channel exchange proceeds via the exchange of the same particles. Thus for \mathcal{D}_u we have the same form as in Eq. (2.18).

In calculating the cross section, we confine ourselves to the situation in which the center of mass system of the incoming particles is at rest relative to the medium. In addition, in this paper, we will examine the cross sections at finite temperature, and in what follows, set the chemical potential to zero. In this case the differential cross section can be written as

$$\frac{d\sigma}{dt} = \frac{1}{16\pi s(s - 4m_u^2)} \frac{1}{4N_c^2} \sum_{s,c} |\mathcal{M}_t - \mathcal{M}_u|^2 \quad . \quad (2.19)$$

For the total cross section, we include a Fermi blocking factor for the final states

$$\sigma = \int dt \frac{d\sigma}{dt} [1 - f_F(\beta\sqrt{s}/2)]^2 \quad , \quad (2.20)$$

with the Fermi function $f_F(x) = 1/(\exp x + 1)$. Note that the total cross section depends only on the temperature T and the center of mass energy \sqrt{s} [9].

The process $uu \rightarrow uu$ is an example of the elastic scattering of quarks that is already present in the $SU_f(2)$ model. It differs from this three flavor calculation in that the additional exchange channels σ_π , η , η' and σ' are missing in that case. For a pure $SU_f(2)$ calculation, only the terms

$$T\mathcal{D}_t^P T = \frac{2G}{1 - 4G\Pi_{u\bar{u}}^P(0, \sqrt{-t})} \quad (2.21a)$$

$$T\mathcal{D}_t^S T = \frac{2G}{1 - 4G\Pi_{u\bar{u}}^S(0, \sqrt{-t})} \quad (2.21b)$$

$$T\mathcal{D}_u^P T = \frac{2G}{1 - 4G\Pi_{u\bar{u}}^P(0, \sqrt{-u})} \quad (2.21c)$$

$$T\mathcal{D}_u^S T = \frac{2G}{1 - 4G\Pi_{u\bar{u}}^S(0, \sqrt{-u})} \quad (2.21d)$$

occur, leading us to the result of Ref. [9]. The appearance of the new exchange channels in both pseudoscalar and scalar sectors leads to a significant enhancement in the numerical values of the cross sections, as will be shown below.

One notes from Table I that the $ud \rightarrow ud$ cross section follows via exchange of the same scalar and pseudoscalar mesons in the t -channel, but a restricted set in the u -channel is admitted. The elastic $ss \rightarrow ss$ processes couple again to the same set of scalar and pseudoscalar mesons in both t - and u -channels. In this case, no coupling to the π or σ_π can occur. When one light and one heavy quark are scattered, one finds that virtual K and σ_K exchanges are possible in the u -channel. This leads to some technical difficulties that are due to the kinematics. One would expect that the kaon (and σ_K) propagator should not depend on the sign of the zero component of the exchanged momentum. This corresponds, via Eqs. (2.8), (2.9), to the condition $\Pi_{q\bar{s}}(p_0, \vec{p}) = \Pi_{q\bar{s}}(-p_0, \vec{p})$, or, through Eqs. (2.10), (2.14), to the equivalent statement

$$B_0(\vec{p}, m_q, \mu_q, m_s, \mu_s, p_0) = B_0(\vec{p}, m_q, \mu_q, m_s, \mu_s, -p_0) \quad . \quad (2.22)$$

However, this symmetry is lost in a straightforward evaluation [17], which is an artifact of our regularization procedure. This can be explicitly traced back to the fact that a shift in variable is performed in certain terms occurring in $\Pi_{q\bar{s}}$. Such

variable shifts are strictly non admissible for divergent integrals, but since they contribute only to order $1/\Lambda$, they are usually ignored. The symmetry condition (2.22) is in any event still fulfilled if the constituent quark masses are equal (i.e. for pions, etas and their scalar partners) or the three momentum argument vanishes. For evaluations in the kaonic sector, however, the violation of (2.22) becomes evident. Accompanying this artifact is the further cutoff and regularization scheme induced artifact that the imaginary part of the polarization is discontinuous at $p_0 = 0$, i.e. at the kinematical point that is required e.g. for the process $u\bar{u} \rightarrow s\bar{s}$ in the center of mass system. We resolve this problem by hand by replacing $B_0(\vec{p}, m_q, \mu_q, m_s, \mu_s, p_0)$ with the symmetric form

$$\frac{1}{2} [B_0(\vec{p}, m_q, \mu_q, m_s, \mu_s, p_0) + B_0(\vec{p}, m_q, \mu_q, m_s, \mu_s, -p_0)] \quad (2.23)$$

whenever dealing with kaons.

2. Numerical Results

Our numerical calculations were performed using the parameter set $m_{0u} = m_{0d} = 5.5$ MeV, $m_{0s} = 140.7$ MeV, $G\Lambda^2 = 1.835$, $K\Lambda^5 = 12.36$ and $\Lambda = 602.3$ MeV. This is the same parameter set that was used in Ref. [8], so the numerical results concerning the static mesonic properties can be obtained from this reference. In particular it was demonstrated in Ref. [8] that at the pionic Mott temperature $T_{M\pi} = 212$ MeV, the pion mass becomes equal to the mass of its constituents $m_\pi = 2m_u$ and the pion becomes a resonant state. The same happens with the kaon at $T_{MK} = 210$ MeV, the η at $T_{M\eta} = 180$ MeV, and the σ at $T_{M\sigma} = 165$ MeV. At these temperatures, the respective particles become unbound. This effect in a rather crude fashion models the deconfinement transition within the NJL model [6].

We first compare our results for three flavors with the corresponding calculation of Ref. [9]. In Fig. 2, we show the total cross section for the process $uu \rightarrow uu$ at $T = 215$ MeV as a function of \sqrt{s} . The temperature chosen lies slightly higher than the pion Mott temperature $T_{M\pi}$; we are therefore in the plasma phase, in which the model may be regarded as physically realistic. As in Ref. [9], our calculations are shown for center of mass energies $\sqrt{s} \leq 2\sqrt{\Lambda^2 + m_u^2}$, i.e. they are restricted by the natural cutoff of this model. Numerically we find that the $SU_f(3)$ calculation yields

a far larger cross section for $uu \rightarrow uu$ than the corresponding two flavor case, the difference being a factor of 3–4. Thus the greater number of exchange channels that become available for three flavors of quarks significantly enhances these scattering processes, and the $SU_f(2)$ result is only recovered on directly eliminating these. The remainder of our calculations are shown for the three flavor sector only.

In Fig. 3, we show the total qq scattering cross sections that involve nonstrange quarks as a function of \sqrt{s} and for two values of the temperature, $T = 215$ MeV and $T = 250$ MeV. The curves for both $uu \rightarrow uu$ and $ud \rightarrow ud$ are essentially flat and display no particular structures. The $ud \rightarrow ud$ scattering cross section lies at a given temperature slightly higher than the $uu \rightarrow uu$ cross section, with both between 1.2 and 1.6 mb for $T = 215$ MeV. This difference can be attributed to the different flavor factors accompanying the various mesonic states. Note that the ud scattering in fact has less exchange mesons available in the u -channel, since no neutral particles are admissible in this channel. As the temperature is increased from $T = 215$ MeV to $T = 250$ MeV, the cross sections become somewhat smaller in magnitude. One also sees that the thresholds for quark quark scattering have shifted to slightly lower values, due to the temperature dependence of the quark masses themselves.

Quark quark scattering processes that involve at least one strange quark are shown in Fig. 4 as a function of \sqrt{s} for the temperatures $T = 215$ MeV and $T = 250$ MeV. The peak like structure in the $us \rightarrow us$ scattering cross section is a cutoff artifact. The cross sections are otherwise featureless. Increasing the temperature from $T = 215$ MeV to $T = 250$ MeV reduces the $us \rightarrow us$ cross section slightly, while raising the $ss \rightarrow ss$ by a small amount.

Differential cross sections may also be calculated for each process. As an example, we show the differential cross section $d\sigma/d\cos\theta$ for the process $ud \rightarrow ud$ as a function of $\cos\theta$ at $\sqrt{s} = 1$ GeV and temperature $T = 250$ MeV in Fig. 5. For comparison, we also include this quantity calculated to lowest order in perturbative QCD and using finite values of the quark masses as are indicated by the NJL model at this temperature. An explicit formulation of the perturbative QCD cross section with finite masses is given in Appendix B. Note that, since these cross sections are infrared divergent at this level, we have introduced an effective gluon mass [18]

$$m_g^2 = 2\pi\alpha_s \left(1 + \frac{N_f}{6}\right) T^2 \approx (600 \text{ MeV})^2 \quad , \quad (2.24)$$

as a regulator, with $N_f = 3$ being the number of flavors here and the QCD coupling strength α_s taken *ad hoc* to be $\alpha_s = 0.6$. The perturbative QCD cross section, which has essentially the same form as the Møller scattering cross section for e^+e^- scattering, displays a strong forward peak. In the limit $m_g \rightarrow 0$, this peak becomes a pole and gives rise to the Coulomb singularity well known from QED. The NJL cross section, on the other hand, also displays a preference for the forward direction. However, this maximum is not as pronounced.

C. Quark Antiquark Scattering

We now turn to a discussion of processes of the form $q\bar{q}' \rightarrow q\bar{q}'$. For these, one has seven independent processes out of a total possible number of fifteen, taking again isospin and charge conjugation symmetry into account. These processes are listed in Table II. The number of independent processes could be further reduced by taking into account crossing symmetry, e.g. by regarding $u\bar{s} \rightarrow u\bar{s}$ and $u\bar{u} \rightarrow s\bar{s}$ as dependent processes. In this paper, however, we regard processes, which are related by crossing symmetry as independent, since crossing symmetry does not lead to numerically equal cross sections. The relevant Feynman diagrams are shown in Fig. 6. Here only s -channel and t -channel diagrams occur. The species of the exchanged mesons are listed in Table II for the independent processes.

As before, we will derive general expressions for the cross sections, illustrating these with the example $u\bar{s} \rightarrow u\bar{s}$.

1. Analytical Calculations

The Feynman diagrams for $q\bar{q}$ scattering are shown in Fig. 6. Analogously to Eqs. (2.15), (2.16), the transition amplitude is given by

$$\begin{aligned} -i\mathcal{M}_s &= \delta_{c_1, c_2} \delta_{c_3, c_4} \bar{v}(p_2) T u(p_1) \left[i\mathcal{D}_s^S(p_1 + p_2) \right] \bar{u}(p_3) T v(p_4) \\ &\quad + \delta_{c_1, c_2} \delta_{c_3, c_4} \bar{v}(p_2) (i\gamma_5 T) u(p_1) \left[i\mathcal{D}_s^P(p_1 + p_2) \right] \bar{u}(p_3) (i\gamma_5 T) v(p_4) \end{aligned} \quad (2.25)$$

$$\begin{aligned} -i\mathcal{M}_t &= \delta_{c_1, c_3} \delta_{c_2, c_4} \bar{u}(p_3) T u(p_1) \left[i\mathcal{D}_t^S(p_1 - p_3) \right] \bar{v}(p_2) T v(p_4) \\ &\quad + \delta_{c_1, c_3} \delta_{c_2, c_4} \bar{u}(p_3) (i\gamma_5 T) u(p_1) \left[i\mathcal{D}_t^P(p_1 - p_3) \right] \bar{v}(p_2) (i\gamma_5 T) v(p_4) \quad . \end{aligned} \quad (2.26)$$

The squares of these amplitudes can again be found in Appendix A.

We illustrate the further calculation by choosing the specific process $u\bar{s} \rightarrow u\bar{s}$. As can be seen from Table II, the s channel of this process proceeds via the exchange of a kaon in the pseudoscalar and a σ_K in the scalar part. This gives

$$T\mathcal{D}_s^PT = 2\mathcal{D}_K \quad (2.27)$$

$$T\mathcal{D}_s^ST = 2\mathcal{D}_{\sigma_K} \quad . \quad (2.28)$$

The t channel proceeds via the exchange of an η or η' in the pseudoscalar, a σ or σ' in the scalar part. This means that we have

$$T\mathcal{D}_t^PT = \frac{4}{3} \frac{\mathcal{K}}{\mathcal{A}\mathcal{C} - \mathcal{B}^2} \left(\mathcal{A} - \frac{1}{\sqrt{2}}\mathcal{B} - \mathcal{C} \right) \quad (2.29)$$

and an analogous expression for the scalar part. The differential cross section is now

$$\frac{d\sigma}{dt} = \frac{1}{16\pi[s - (m_u + m_s)^2][s - (m_u - m_s)^2]} \frac{1}{4N_c^2} \sum_{s,c} |\mathcal{M}_s - \mathcal{M}_t|^2 \quad (2.30)$$

and the total cross section is calculated as

$$\sigma = \int dt \frac{d\sigma}{dt} [1 - f_F(\beta E_3)] [1 - f_F(\beta E_4)] \quad , \quad (2.31)$$

where a Fermi blocking factor for the final states has been introduced. In Eq. (2.31), $E_i^2 = p_i^2 + m_i^2$, where $i = 3, 4$.

2. Numerical Results

In Fig. 7, we show a comparison of the scattering cross sections calculated in $SU_f(3)$ with the corresponding calculation in $SU_f(2)$, for a specific process $u\bar{d} \rightarrow u\bar{d}$, at the temperature $T = 215$ MeV. In contrast to the comparison shown in Fig. 2 for quark quark scattering, the difference, on this scale, is not so great. This is due to the fact that the $q\bar{q}$ scatterings are resonance dominated: The temperature chosen lies only slightly higher than the pionic and kaonic Mott temperatures $T_{M\pi} = 212$ MeV and $T_{MK} = 210$ MeV, so that both pions and kaons appear as very sharp resonances in the reactions containing them, see Table II. We therefore find that large cross sections occur at threshold for the process shown, in this case due to the pion resonance. We next show all $q\bar{q}$ cross sections that contain no strange quarks or

antiquarks in the incoming channel as a function of \sqrt{s} at the temperature $T = 215$ MeV in Fig. 8. These cross sections all display pronounced structures, especially in comparison with the quark quark scatterings of similar flavor (cf. Fig. 3), as they admit resonances in the s -channel. Cross sections with $u\bar{u}$ in the initial state are in addition enhanced by the presence of σ mesons. By contrast, the $u\bar{u} \rightarrow s\bar{s}$ reaction contains no resonant structure and remains of the order of 1 mb over its range in \sqrt{s} . At the Mott temperature itself, intermediate states in the s -channel give rise to infinite cross sections at threshold. This feature, which also appears in other processes like $\pi\pi \rightarrow \pi\pi$ [19], $\pi\gamma \rightarrow \pi\gamma$ [20] or $q\bar{q} \rightarrow \gamma\gamma$ [21], is akin to the phenomenon of critical opalescence and has been discussed in greater detail in Ref. [6]. For temperatures above the Mott transition, such as the one shown in this figure, the cross sections are large but finite at threshold. Increasing the temperature further to $T = 250$ MeV, as has been done for the same set of reactions in Fig. 9, shows that the resonances have become broader and the cross sections in this regime smaller. Nevertheless, this melting of the pion and sigma resonances still leads to cross sections that are highly enhanced over a range of \sqrt{s} between 0.2 and 0.8 GeV in comparison with other scattering processes, where cross sections of only $\mathcal{O}(1 \text{ mb})$ are found. This remnant of the critical scattering phenomenon is thus still strongly visible even at high temperatures. Although it is not possible to observe such scatterings directly in experiment, it may lead to observable consequences when embedded in a consistently constructed chiral transport theory.

In Fig. 10, we show the scattering cross sections for quarks and antiquarks for processes that contain at least one strange particle in the incoming channel at $T = 215$ MeV. The threshold behavior is strongly dominated by the resonant structure for the case of the process $u\bar{s} \rightarrow u\bar{s}$. Here an exchanged kaon gives the dominant resonance, with a shoulder due to the σ_K . The $s\bar{s} \rightarrow u\bar{u}$ singularity seen is a kinematical singularity, that arises because the reaction is exothermic. The $s\bar{s} \rightarrow s\bar{s}$ displays no pronounced resonance – there is a small one due to the σ' or η' . At a somewhat higher temperature, $T = 250$ MeV, the resonant structure that forms a remnant of critical scattering for $u\bar{s} \rightarrow u\bar{s}$, has become smaller and broader. Once again, it still peaks at 15 mb over a range of \sqrt{s} between 0.4 and 1 GeV, and may therefore also lead to an observable effect when embedded in a consistent transport theory.

Figure 12 shows the differential cross section for the process $u\bar{s} \rightarrow u\bar{s}$, given as function of $\cos\theta$. Whereas the one gluon exchange perturbative QCD cross section, see Appendix B, once again resembles Møller scattering for e^+e^- and is strongly peaked in the forward direction, the NJL cross section is flat. This comes about due to the dominance of the s -channel exchange at this energy, which proceeds via spinless particles and thus shows no anisotropy.

III. TRANSPORT PROPERTIES

A. Averaged Transition Rates

To calculate the transport coefficients, we need averaged transition rates. These are expressed as [8]

$$\bar{w}(T) = \frac{1}{\rho_1(T)\rho_2(T)} \int \frac{d^3p_1}{(2\pi)^3} \frac{d^3p_2}{(2\pi)^3} [2N_c f_F(\beta E_1)] [2N_c f_F(\beta E_2)] w(s, T) \quad , \quad (3.1)$$

in terms of the transition rate $w(s, T)$, which in turn is defined as the product of cross section and relative velocity:

$$w(s, T) = |\vec{v}_{\text{rel}}| \sigma(s, T) \quad (3.2)$$

$$|\vec{v}_{\text{rel}}| = \frac{\sqrt{(p_1 p_2)^2 - m_1^2 m_2^2}}{E_1 E_2} \quad . \quad (3.3)$$

The quark density in Eq. (3.1) is defined as the integral of the Fermi distribution function over all momenta:

$$\rho_f(T) = \int \frac{d^3p}{(2\pi)^3} 2N_c f_F(\beta \sqrt{p^2 + m_f^2}) \quad . \quad (3.4)$$

To evaluate Eq. (3.1), we make the approximation that the total cross section is only a function of s , even if the incoming pair is moving with respect to the medium. In this case the averaged transition rate can be expressed as

$$\bar{w}(T) = \int_{(m_1+m_2)^2}^{\infty} ds \sqrt{(p_1 p_2)^2 - (m_1 m_2)^2} \sigma(s, T) P(s, T) \quad , \quad (3.5)$$

where the weight function $P(s, T)$ is given as

$$P(s, T) = \frac{1}{\rho_1(T)\rho_2(T)} \frac{1}{16\pi^4} \int_{m_1}^{\infty} dE_1 [2N_c f_F(\beta E_1)] \quad (3.6)$$

$$\times \int_{m_2}^{\infty} dE_2 [2N_c f_F(\beta E_2)] \Theta(4|\vec{p}_1|^2 |\vec{p}_2|^2 - (s - (m_1^2 + m_2^2) - 2E_1 E_2)^2) \quad .$$

This weight function is illustrated in Fig. 13 for $m_1 = m_2 = m_u$, and the two values of the temperature $T = 215$ MeV and $T = 250$ MeV. One sees that this function weights the lower energies strongly and has an exponential tail at a given temperature. Increasing the temperature from $T = 215$ MeV to $T = 250$ MeV has the consequence that the peak value of the weight function is shifted and reduced somewhat and the exponential decay is weaker. Note that this approach differs from that taken in Ref. [9] in that $P(s, T)$ in Eq. (3.6) is *not* a normalized probability distribution. In Fig. 14, we show the averaged transition rates for the quark quark scattering processes $uu \rightarrow uu$ and $ud \rightarrow ud$ together with the quark antiquark scattering processes $u\bar{d} \rightarrow u\bar{d}$ and $u\bar{s} \rightarrow u\bar{s}$. We see that the quark antiquark scattering averaged rates lie higher than the quark quark scattering ones. There is a sudden rise in the quark antiquark rates as one moves through the Mott temperatures. This is due to the inclusion of resonance channels at and above this point. Above the Mott temperatures, in the region of interest, both are decreasing with temperature.

B. Thermal Relaxation Times

Since the definition of the averaged transition rate strongly resembles the collision integral of a Boltzmann equation [22], we can immediately identify the thermal relaxation time for each species as

$$\tau_f^{-1} = \sum_{f'} \rho_{f'} \bar{w}_{ff'} \quad , \quad (3.7)$$

where the summation runs over all quark species and \bar{w}_{fg} is the sum of the transition rates of all processes with species f and g in the initial state. Our numerical calculation for $\tau_u = \tau_d$ and τ_s is shown as a function of temperature in Fig. 15. The temperature region below $T_{M\pi}$ is of purely academic interest, since physically there should be no free quarks: we show it here for completeness. The relaxation time is large for small temperatures, which is due to the low quark density. In the physically interesting region $T \geq T_{M\pi}$, we obtain relaxation times of the order of 1–1.3 fm/c

for light quarks and 1.3–2 fm/ c for strange quarks for temperatures greater than the pion Mott temperature.

C. Mean Free Path

We define the mean free path of a particle as [23]

$$\lambda_f = \bar{v}_f \tau_f \quad , \quad (3.8)$$

where the mean velocity of flavor f is given as

$$\bar{v}_f = \frac{2N_c}{\rho_f} \int \frac{d^3p}{(2\pi)^3} \frac{p}{E_f} f_F(\beta E_f) \quad . \quad (3.9)$$

Our numerical calculation for λ is shown in Fig. 16. Once again, we also show the low temperature region, although, as already pointed out, this is unphysical; one can therefore regard the physical mean free path as being the value obtained in the high temperature regime. For high temperatures, $T \gg m_f$, one finds $\lambda_f \approx \tau_f$, since \bar{v}_f is approximately equal to one for all flavors, as can be seen from Eq. (3.9). For lower temperatures, $\bar{v}_s < \bar{v}_u < 1$, causing the curves in Fig. 16 to lie closer together than the corresponding two curves of Fig. 15. From Fig. 16, we obtain a mean free path of 0.9–1.4 fm for light quarks and 1.1–1.6 fm for strange quarks.

D. Viscosity

To a first approximation, the shear viscosity is proportional to the mean free path [9,23,24]:

$$\eta_f = \frac{4}{15} \rho_f \bar{p}_f \lambda_f \quad , \quad (3.10)$$

where \bar{p}_f is the mean momentum for a quark of flavor f :

$$\bar{p}_f = \frac{2N_c}{\rho_f} \int \frac{d^3p}{(2\pi)^3} p f_F(\beta E_f) \quad . \quad (3.11)$$

A more detailed analysis [23] shows that in averaging the cross sections, large scattering angles should be preferred, which is achieved by replacing the total cross section implicitly contained in Eq. (3.10) with the weighted average

$$\sigma \rightarrow \sigma_\eta = \int d\Omega \frac{d\sigma}{d\Omega} \sin^2 \theta [1 - f_F(\beta E_3)][1 - f_F(\beta E_4)] \quad . \quad (3.12)$$

Since in a first approximation, η should be proportional to T^3 , we show $\eta_u/T^3 = \eta_d/T^3$ and η_s/T^3 in Fig. 17. Since the mean free path for all flavors is approximately equal, the difference in the curves is mainly a density effect. Beyond the Mott transition, the result for η/T^3 lies in the range 0.83–1.0 for light quarks and 0.68–0.75 for strange quarks. The total viscosity, calculated for two flavors, amounts to

$$3.2 < \eta/T^3 < 4.0 \quad (3.13)$$

and

$$4.6 < \eta/T^3 < 5.5 \quad (3.14)$$

for three flavors. The value for two flavors lies under that given in Ref. [9]. This is a direct manifestation of the difference in the cross sections shown in Fig. 2 for two and three flavors, due to the additional channels that are available in the three flavor calculation. A classical hydrodynamical estimate [12] places loose bounds on this number,

$$2 \leq \eta/T^3 \leq 3\tau T \quad , \quad (3.15)$$

in which τ is the proper time for the expansion of the system. For $\tau \approx 5 \text{ fm}/c$, our values for the total viscosity lie within these bounds, but are smaller than those calculated in this hydrodynamical approach, which gives $\eta/T^3 \approx 10$ [12]. Alternatively, perturbative QCD calculations have been performed [10,11] for this quantity. The variational perturbative calculation of [10] places a lower bound on η as being

$$\eta/T^3 \geq -\frac{1.16}{\alpha_s^2 \log \alpha_s} \quad . \quad (3.16)$$

For $\alpha_s = 0.6$, this is 6.3, which is slightly higher than our result. Technically this comes about from the fact that the perturbative QCD calculation favors forward scattering, while the NJL model allows for a softer angular distribution. The perturbative QCD result may however be substantially altered in the non-perturbative region, so we do not regard this as being a serious discrepancy.

IV. STRANGENESS ENHANCEMENT

Given the elastic scattering cross sections, we are able to address the problem of strangeness enhancement in a quark meson plasma within our model. We choose an approach similar to that taken in Refs. [13,25,26]. However, instead of discussing gluon exchange, we compute the contribution of the exchange of mesonic resonances.

The strangeness changing processes, which we have considered in this work, are

$$u\bar{u} \rightarrow s\bar{s} \qquad d\bar{d} \rightarrow s\bar{s} \qquad (4.1)$$

and the respective back reactions

$$s\bar{s} \rightarrow u\bar{u} \qquad s\bar{s} \rightarrow d\bar{d} \quad . \qquad (4.2)$$

In the following, we consider the light quarks to be fully equilibrated. We discuss two possible definitions of the chemical relaxation time. The first one is defined as the number of strange quarks present in chemical equilibrium, divided by the number of strange quarks produced per unit time:

$$\tau_1 = \frac{\rho_s^{\text{eq}}}{2\rho_u\rho_{\bar{u}}\bar{w}_{u\bar{u} \rightarrow s\bar{s}}} \quad . \qquad (4.3)$$

The factor 2 in this expression accounts for the number of light quark flavors, which give equal contributions. This quantity is comparable with that given in Ref. [13]. In this case one has, as a first approximation,

$$\rho_s(t) = \rho_s^{\text{eq}} \tanh(t/\tau_1) \quad . \qquad (4.4)$$

The second definition of the strange quark relaxation time is

$$\tau_2 = \frac{1}{2\rho_{\bar{u}}\bar{w}_{u\bar{u} \rightarrow s\bar{s}}} \quad . \qquad (4.5)$$

Again, the factor 2 counts the light quark flavors. This corresponds to making the rate equation ansatz

$$\frac{d\rho_s}{dt} = \frac{1}{\tau_2}\rho_u \quad , \qquad (4.6)$$

neglecting the back reaction. The two definitions of τ_1 and τ_2 differ by the factor $\rho_s^{\text{eq}}(T)/\rho_u(T)$, which is smaller than one since $m_s(T) > m_u(T)$, but approaches one for temperatures $T \gg m_s$.

By contrast, in Ref. [13], the strangeness relaxation time was found within the framework of perturbative QCD to be dominated by the process $gg \rightarrow s\bar{s}$. For this process, these authors obtained

$$\tau_{gg} = \frac{1.61 (m_s/T) \exp(m_s/T)}{\alpha_s^2 T (1 + \frac{99}{56} T/m_s + \dots)} \quad , \quad (4.7)$$

where α_s is the strong coupling constant, which was assumed to be 0.6 for all temperatures. The relaxation time due to the processes (4.1) was calculated by the same authors to be roughly a factor of 10 larger.

Our numerical calculation of τ_1 , τ_2 and τ_{gg} from Eqs. (4.3), (4.5) and (4.7) are shown in Fig. 18. Of interest in this figure are the curves in the temperature range $T > T_{M\pi}$. The solid curve shows τ_1 , which lies in the range 11-17 fm/c, whereas τ_2 , indicated by the dashed line, lies in the range 16–30 fm/c. The relaxation time due to gluon–gluon collisions, as given in Ref. [13], is given by the dot–dashed line and is clearly seen to be considerably smaller than τ_1 . However, according to Ref. [13], this calculation assumes a temperature independent value for the strange quark mass of $m_s = 150$ MeV. The NJL model, on the other hand, predicts a strange quark mass, which, even at high temperatures, is at least twice as large as the current quark mass value of 150 MeV [8]. In the temperature range shown in the figure, $150 \text{ MeV} < T < 250 \text{ MeV}$, the strange quark mass falls from $510 \text{ MeV} > m_s > 380 \text{ MeV}$. At the pion Mott temperature $T_{M\pi} = 212 \text{ MeV}$, we have $m_s = 415 \text{ MeV}$. An evaluation of Eq. (4.7) with masses according to the NJL gap equation (2.7) is indicated by the dotted curve in Fig. 18. Since the chemical relaxation time in Eq. (4.7) depends exponentially on m_s , an exact knowledge of this quantity is essential, as can be seen by comparing the dot–dashed and the dotted curve in Fig. 18. Taking the strange quark mass from the NJL gap equation gives a τ_{gg} of the order of τ_1 . Furthermore, Eq. (4.7) relies on the assumption, that light quarks and gluons are massless above the phase transition. Finite light quark and gluon masses could also shift the chemical relaxation times.

Experimentally, the strangeness content of the observed mesons is parametrized in the ratio

$$r_{\text{ex}} = \frac{4 \langle K_S^0 \rangle}{3 \langle \pi^- \rangle} \quad , \quad (4.8)$$

where $\langle K_S^0 \rangle$ and $\langle \pi^- \rangle$ are the mean multiplicities of the observed mesons. At 200 GeV/nucleon the experimental values are [27]

$$r_{\text{ex}} = \begin{cases} (8.7 \pm 1.3)\% & N + N \\ (15.4 \pm 2.6)\% & S + S \end{cases} . \quad (4.9)$$

These values should be compared with the thermal value

$$r_{\text{th}} = \frac{\rho_s^{\text{eq}}(T)}{\rho_u(T) + \rho_d(T)} = 27\% \quad (4.10)$$

at $T = 200$ MeV. If we interpret the increase from r_{ex}^{N+N} to r_{ex}^{S+S} as being due to an “chemical equilibration” within the quark plasma alone, we can determine the time t_0 available for equilibration from the equation

$$\tanh\left(\frac{t_0}{\tau_1}\right) = \frac{r_{\text{ex}}^{S+S} - r_{\text{ex}}^{N+N}}{r_{\text{th}}} , \quad (4.11)$$

and one obtains $t_0 \approx \tau_1/4 \approx 4$ fm/ c . This value is clearly an upper limit, since strangeness can also be created within the hadronization process (found to contribute around 1% in our previous calculation [8]) and in the hadronic gas. This would mean that one has to assume a plasma lifetime of less than 4 fm/ c . Note that calculations using the hydrodynamical Landau model [15], indicate that the total lifetime of the fireball (plasma + hadronization + hadron gas) is of the order of 5 fm/ c for $S + S$ collisions. This is not in contradiction with our estimate.

V. GENERAL DISCUSSION

In this section, we discuss general features relating to our calculation and its philosophy. We have evaluated the quark self energy in the Hartree approximation, which corresponds to the leading order term in a $1/N_c$ approximation. The $1/N_c$ expansion is necessary in order to have a well-defined method of dealing with a strong coupling theory. Concomitantly, the pion masses are calculated in the random phase approximation (RPA), which, taken together with the quark self energy, can be shown to form a consistent expansion in a chiral sense – i.e. the Goldstone mode is guaranteed in the chiral limit. The masses are not shown explicitly here – the calculation is standard and has been given in Refs. [6,8,28] in detail. In particular, to this level of approximation, the quark self energy is always real, even in a thermal medium, while the mesonic self energies are complex, depending on various parameters.

Given this circumstance, we have calculated quark–quark and quark–antiquark scattering processes. In a simplistic fashion, by analogy with the Boltzmann equation, we are able to extract transport coefficients, and in particular, lifetimes, which have been discussed in detail in Section III. These lifetimes imply of course that the u , d and s quarks carry widths that are inversely proportional to these. Thus one sees, that, while this is a consistent chiral and $1/N_c$ expansion, it is *not* a self-consistent calculation of the *widths*. In order to do so, one must go *beyond* the lowest order $1/N_c$ calculation. Several attempts to do this [7] and also to include finite temperature [29] have difficulties either in including all possible terms, and/or maintaining chiral symmetry. A first calculation [30] that attempts to go further and calculate the quark widths self-consistently ignores the consistent calculation of the meson sector, and thus violates chiral symmetry requirements at this level. We find that our widths $\sim 1/\tau$ are of the order of 200 MeV and lie somewhat below the values quoted in Ref. [30].

In this discussion, we wish to point out that there are contradicting expansions that one can examine. It has always been a fixed tenet of transport theory that truncations should be energy and *symmetry* conserving, and we have thus based our calculation on this. Clearly more work is required to incorporate the higher order terms in a self-consistent fashion that can also determine quark widths in medium simultaneously. As such, we can at best regard our transport theory results as estimates that may be compared with other similarly made estimates.

Finally it is perhaps worth commenting that the correct inclusion of the quasi particles with widths is extremely important. In the calculation of Ref. [31], the authors have found that a consistent treatment of the widths leads to a correction of a factor of two for the collision rates. In addition, a consistent treatment may alter the transport coefficients substantially, when calculated field theoretically [32,33]. The imaginary part of the self energy can also be shown to be connected with memory effects [34].

In concluding this section, it is evident that, within the NJL model, an expansive study that constructs a transport theory that accounts for all these problems, still requires substantial development. A first formal attempt at this has been made in Refs. [35,36].

VI. SUMMARY AND CONCLUSIONS

We have examined the finite temperature behavior of elastic scattering processes of quarks with quarks and quarks with antiquarks within an effective three flavor model in which chiral symmetry is regarded as the most important underlying feature. In the quark quark elastic scattering, we have seen that the three flavor calculation differs quite substantially from a calculation that accounts for two flavors only, due to the influence of additional channels. The quark quark scattering cross sections are enhanced by a factor of 3–4, but are otherwise featureless. On the other hand the quark antiquark scattering cross sections display divergencies at the Mott temperature, which we can regard as an indication of critical scattering. At temperatures between $T_{M\pi}$ and $T = 250$ MeV, the remnants of the critical scattering, i.e. resonant structures that occur in the s -channel, are clearly visible and enhance the cross sections substantially in comparison with the background. Such a feature, it is hoped, may be visible in a final analysis that involves a consistent transport theory. The differential cross sections that we have calculated are found to be of the same order of magnitude as perturbative QCD calculations, in which a gluon mass of $m_g = 600$ MeV and a strong coupling constant of $\alpha_s = 0.6$ have been assumed.

We have also examined transport coefficients in the $SU_f(3)$ model. We find thermal relaxation times of 1–1.3 fm/ c for light quarks and 1.3–2 fm/ c for strange quarks. The mean free paths lie in similar ranges, being 0.9–1.4 fm and 1.1–1.6 fm for light and strange quarks respectively. The ratios of the viscosity to the third power of the temperature, η/T^3 per quark flavor, fall between 0.83–1.0 and 0.68–0.75 for light and strange quarks respectively. The total viscosity coefficient for two flavors is found to be a factor roughly two smaller than previous $SU_f(2)$ calculations. This is attributable to the enhanced cross sections that enter into this $SU_f(3)$ calculation. Our value still falls within the bracketed range given by hydrodynamic estimates, while being slightly less than the perturbative QCD result.

In studying strangeness enhancement due to the possible strangeness changing reactions that occur via quark antiquark annihilation, we find that relaxation times are considerably larger than those derived from perturbative QCD with the naive assumption $m_s = 150$ MeV. In the NJL model, $m_s = m_s(T)$ is a function of temperature and its value lies significantly higher than the current quark mass value

$m_s \approx 150$ MeV over the entire temperature range of interest. This feature follows from earlier temperature studies of the dynamically generated quark masses [8]. If one recalculates the perturbative QCD expression using the temperature dependent NJL quark masses, one arrives at chemical relaxation times that are of the same order as our calculation. In attempting to assess the relevance of elastic scattering processes on strangeness production in heavy ion collisions, we note that this is a sensitive function of the plasma lifetime. A plasma lifetime of the order of 4 fm/ c would allow one to account for all of the observed strangeness enhancement in $S+S$ collisions via the mechanism of elastic scattering. Since the plasma lifetime probably lies below this value, other processes such as hadronization and final state interactions must also play a role.

ACKNOWLEDGMENTS

We wish to thank P. Zhuang and D. Blaschke for illuminating discussions. This work has been supported in part by the Deutsche Forschungsgemeinschaft under contract no. Hu 233/4–3, by the Federal Ministry for Education and Research, under contract no. 06 HD 742.

APPENDIX A: SQUARED TRANSITION AMPLITUDES

1. Quark Quark Scattering

The matrix elements in Eqs. (2.15) and (2.16) have the form

$$\begin{aligned} -i\mathcal{M}_t &= \delta_{c_1,c_3}\delta_{c_2,c_4}\bar{u}(p_3)u(p_1)\left[i\mathcal{D}_t^S(p_1-p_3)\right]\bar{u}(p_4)u(p_2) \\ &\quad + \delta_{c_1,c_3}\delta_{c_2,c_4}\bar{u}(p_3)(i\gamma_5)u(p_1)\left[i\mathcal{D}_t^P(p_1-p_3)\right]\bar{u}(p_4)(i\gamma_5)u(p_2) \end{aligned} \quad (\text{A1})$$

and

$$\begin{aligned} -i\mathcal{M}_u &= \delta_{c_1,c_4}\delta_{c_2,c_3}\bar{u}(p_4)u(p_1)\left[i\mathcal{D}_u^S(p_1-p_4)\right]\bar{u}(p_3)u(p_2) \\ &\quad + \delta_{c_1,c_4}\delta_{c_2,c_3}\bar{u}(p_4)(i\gamma_5)u(p_1)\left[i\mathcal{D}_u^P(p_1-p_4)\right]\bar{u}(p_3)(i\gamma_5)u(p_2) \quad . \end{aligned} \quad (\text{A2})$$

Here we have dropped the T factors for simplicity, since they can easily be included by a rescaling of the propagators. After a short calculation, one obtains

$$\begin{aligned} \frac{1}{4N_c^2} \sum_{s,c} |\mathcal{M}_t|^2 &= \frac{1}{4} \left\{ \left| \mathcal{D}_t^S \right|^2 \text{tr}[(\not{p}_3 + m_3)(\not{p}_1 + m_1)] \text{tr}[(\not{p}_4 + m_4)(\not{p}_2 + m_2)] \right. \\ &\quad \left. + \left| \mathcal{D}_t^P \right|^2 \text{tr}[(\not{p}_3 + m_3)\gamma_5(\not{p}_1 + m_1)\gamma_5] \text{tr}[(\not{p}_4 + m_4)\gamma_5(\not{p}_2 + m_2)\gamma_5] \right\} . \end{aligned} \quad (\text{A3})$$

The interference term between the scalar and pseudoscalar part vanishes. The final result can be expressed using the Mandelstam variable t :

$$\frac{1}{4N_c^2} \sum_{s,c} |\mathcal{M}_t|^2 = \left| \mathcal{D}_t^S \right|^2 t_{13}^+ t_{24}^+ + \left| \mathcal{D}_t^P \right|^2 t_{13}^- t_{24}^- , \quad (\text{A4})$$

where we have abbreviated $t_{ij}^\pm = t - (m_i \pm m_j)^2$. Analogously, one obtains

$$\frac{1}{4N_c^2} \sum_{s,c} |\mathcal{M}_u|^2 = \left| \mathcal{D}_u^S \right|^2 u_{14}^+ u_{23}^+ + \left| \mathcal{D}_u^P \right|^2 u_{14}^- u_{23}^- , \quad (\text{A5})$$

with $u_{ij}^\pm = u - (m_i \pm m_j)^2$. For the interference term, the spin summation results in

$$\begin{aligned} \frac{1}{4N_c^2} \sum_{s,c} \mathcal{M}_t \mathcal{M}_u^* &= \frac{1}{4N_c} \left\{ \mathcal{D}_t^S \mathcal{D}_u^{S*} \text{tr}[(\not{p}_3 + m_3)(\not{p}_1 + m_1)(\not{p}_4 + m_4)(\not{p}_2 + m_2)] \right. \\ &\quad - \mathcal{D}_t^S \mathcal{D}_u^{P*} \text{tr}[(\not{p}_3 + m_3)(\not{p}_1 + m_1)\gamma_5(\not{p}_4 + m_4)(\not{p}_2 + m_2)\gamma_5] \\ &\quad - \mathcal{D}_t^P \mathcal{D}_u^{S*} \text{tr}[(\not{p}_3 + m_3)\gamma_5(\not{p}_1 + m_1)(\not{p}_4 + m_4)\gamma_5(\not{p}_2 + m_2)] \\ &\quad \left. + \mathcal{D}_t^P \mathcal{D}_u^{P*} \text{tr}[(\not{p}_3 + m_3)\gamma_5(\not{p}_1 + m_1)\gamma_5(\not{p}_4 + m_4)\gamma_5(\not{p}_2 + m_2)\gamma_5] \right\} \\ &= \frac{1}{4N_c} \left[\mathcal{D}_t^S \mathcal{D}_u^{S*} (t_{13}^+ t_{24}^+ - s_{12}^+ s_{34}^+ + u_{14}^+ u_{23}^+) \right. \\ &\quad - \mathcal{D}_t^S \mathcal{D}_u^{P*} (t_{13}^+ t_{24}^+ - s_{12}^- s_{34}^- + u_{14}^- u_{23}^-) \\ &\quad - \mathcal{D}_t^P \mathcal{D}_u^{S*} (t_{13}^- t_{24}^- - s_{12}^- s_{34}^- + u_{14}^+ u_{23}^+) \\ &\quad \left. + \mathcal{D}_t^P \mathcal{D}_u^{P*} (t_{13}^- t_{24}^- - s_{12}^+ s_{34}^+ + u_{14}^- u_{23}^-) \right] . \end{aligned} \quad (\text{A6})$$

Here, we have abbreviated $s_{ij}^\pm = s - (m_i \pm m_j)^2$. If the masses of all incoming and outgoing particles are equal, Eqs. (A4)–(A6) can be largely simplified to yield

$$\frac{1}{4N_c^2} \sum_{s,c} |\mathcal{M}_t|^2 = \left| \mathcal{D}_t^S \right|^2 (t - 4m^2)^2 + \left| \mathcal{D}_t^P \right|^2 t^2 , \quad (\text{A7})$$

$$\frac{1}{4N_c^2} \sum_{s,c} |\mathcal{M}_u|^2 = \left| \mathcal{D}_u^S \right|^2 (u - 4m^2)^2 + \left| \mathcal{D}_u^P \right|^2 u^2 , \quad (\text{A8})$$

and

$$\begin{aligned} \frac{1}{4N_c^2} \sum_{s,c} \mathcal{M}_t \mathcal{M}_u^* &= -\frac{1}{2N_c} \left\{ \mathcal{D}_t^S \mathcal{D}_u^{S*} [tu + 4m^2(t + u) - 16m^4] \right. \\ &\quad \left. - \mathcal{D}_t^S \mathcal{D}_u^{P*} u(t - 4m^2) - \mathcal{D}_t^P \mathcal{D}_u^{S*} t(u - 4m^2) + \mathcal{D}_t^P \mathcal{D}_u^{P*} tu \right\} , \end{aligned} \quad (\text{A9})$$

which is the result of Ref. [9].

2. Quark Antiquark Scattering

The matrix elements for $q\bar{q}$ scattering are

$$\begin{aligned} -i\mathcal{M}_s &= \delta_{c_1, c_2} \delta_{c_3, c_4} \bar{v}(p_2) u(p_1) \left[i\mathcal{D}_s^S(p_1 + p_2) \right] \bar{u}(p_3) v(p_4) \\ &\quad + \delta_{c_1, c_2} \delta_{c_3, c_4} \bar{v}(p_2) (i\gamma_5) u(p_1) \left[i\mathcal{D}_s^P(p_1 + p_2) \right] \bar{u}(p_3) (i\gamma_5) v(p_4) \end{aligned} \quad (\text{A10})$$

and

$$\begin{aligned} -i\mathcal{M}_t &= \delta_{c_1, c_3} \delta_{c_2, c_4} \bar{u}(p_4) u(p_1) \left[i\mathcal{D}_t^S(p_1 - p_3) \right] \bar{v}(p_3) v(p_2) \\ &\quad + \delta_{c_1, c_3} \delta_{c_2, c_4} \bar{u}(p_4) (i\gamma_5) u(p_1) \left[i\mathcal{D}_t^P(p_1 - p_3) \right] \bar{v}(p_3) (i\gamma_5) v(p_2) \quad . \end{aligned} \quad (\text{A11})$$

The square of these matrix elements can be immediately written down by using the fact that the crossing transformation

$$\begin{aligned} p_1 &\rightarrow p_1 & p_2 &\rightarrow -p_4 \\ p_3 &\rightarrow -p_2 & p_4 &\rightarrow p_3 \end{aligned} \quad (\text{A12})$$

transforms the t (u) channel of qq scattering to the s (t) channel for $q\bar{q}$ scattering.

Thus one obtains

$$\frac{1}{4N_c^2} \sum_{s,c} |\mathcal{M}_s|^2 = \left| \mathcal{D}_s^S \right|^2 s_{12}^+ s_{34}^+ + \left| \mathcal{D}_s^P \right|^2 s_{12}^- s_{34}^- \quad , \quad (\text{A13})$$

$$\frac{1}{4N_c^2} \sum_{s,c} |\mathcal{M}_t|^2 = \left| \mathcal{D}_t^S \right|^2 t_{13}^+ t_{24}^+ + \left| \mathcal{D}_t^P \right|^2 t_{13}^- t_{24}^- \quad , \quad (\text{A14})$$

and

$$\begin{aligned} \frac{1}{4N_c^2} \sum_{s,c} \mathcal{M}_s \mathcal{M}_t^* &= \frac{1}{4N_c} \left[\mathcal{D}_s^S \mathcal{D}_t^{S*} \left(s_{12}^+ s_{34}^+ - u_{14}^+ u_{24}^+ + t_{13}^+ t_{24}^+ \right) \right. \\ &\quad - \mathcal{D}_s^S \mathcal{D}_t^{P*} \left(s_{12}^+ s_{34}^+ - u_{14}^- u_{24}^- + t_{13}^- t_{24}^- \right) \\ &\quad - \mathcal{D}_s^P \mathcal{D}_t^{S*} \left(s_{12}^- s_{34}^- - u_{14}^- u_{24}^- + t_{13}^+ t_{24}^+ \right) \\ &\quad \left. + \mathcal{D}_s^P \mathcal{D}_t^{P*} \left(s_{12}^- s_{34}^- - u_{14}^+ u_{24}^+ + t_{13}^- t_{24}^- \right) \right] \quad . \end{aligned} \quad (\text{A15})$$

Again, these expressions can be greatly simplified in the case of equal quark masses.

APPENDIX B: ELASTIC SCATTERING IN PERTURBATIVE QCD

In perturbative QCD, the elastic scattering of quarks and antiquarks proceeds in lowest order via one gluon exchange. A previous calculation for the case of massless quarks and gluons has been given in Ref. [37]. Here we extend this result to the case of three flavors and introduce finite masses for quarks and gluons.

1. Quark Quark Scattering

The elastic scattering of two quarks of flavor f and f' proceeds via a t -channel exchange, if $f \neq f'$, and via t - and u -channel exchanges if $f = f'$. The differential cross section is

$$\frac{d\sigma}{dt} = \frac{1}{16\pi[s - (m_f - m_{f'})^2][s - (m_f + m_{f'})^2]} \frac{1}{4N_c^2} \sum_{s,c} |\mathcal{M}_t - \delta_{f,f'} \mathcal{M}_u|^2 \quad . \quad (\text{B1})$$

For the t -channel exchange, one has, using the Feynman gauge,

$$-i\mathcal{M}_t = \bar{u}(p_3) \left(-ig_s \gamma^\mu \frac{1}{2} \lambda_{ij}^a \right) u(p_1) \frac{-i\delta_{ab} g_{\mu\nu}}{t - m_g^2} \bar{u}(p_4) \left(-ig_s \gamma^\nu \frac{1}{2} \lambda_{kl}^b \right) u(p_2) \quad , \quad (\text{B2})$$

where we have introduced a finite gluon mass m_g in order to avoid Coulomb singularities. For the u -channel, one obtains

$$-i\mathcal{M}_u = \bar{u}(p_3) \left(-ig_s \gamma^\mu \frac{1}{2} \lambda_{il}^a \right) u(p_2) \frac{-i\delta_{ab} g_{\mu\nu}}{u - m_g^2} \bar{u}(p_4) \left(-ig_s \gamma^\nu \frac{1}{2} \lambda_{kj}^b \right) u(p_1) \quad . \quad (\text{B3})$$

Using standard techniques, the expression

$$\begin{aligned} \frac{1}{4N_c^2} \sum_{s,c} |\mathcal{M}_t - \delta_{f,f'} \mathcal{M}_u|^2 &= \frac{64\pi^2 \alpha_s^2}{9} \left[\frac{2(s - m_f^2 - m_{f'}^2)^2 + t^2 + 2st}{(t - m_g^2)^2} \right. \\ &\quad + \delta_{f,f'} \frac{2(s - 2m_f^2)^2 + u^2 + 2su}{(u - m_g^2)^2} \\ &\quad \left. - \frac{2}{3} \delta_{f,f'} \frac{(s - 4m_f^2)^2 - 4m_f^4}{(t - m_g^2)(u - m_g^2)} \right] \end{aligned} \quad (\text{B4})$$

can be derived, where $\alpha_s = g_s^2/(4\pi)$ is the QCD fine structure constant.

2. Quark Antiquark Scattering

In the case of different incoming flavors, elastic scattering proceeds via a t -channel exchange. In this case, we have

$$\frac{d\sigma}{dt} = \frac{1}{16\pi[s - (m_f - m_{f'})^2][s - (m_f + m_{f'})^2]} \frac{1}{4N_c^2} \sum_{s,c} |\mathcal{M}_t|^2 \quad , \quad (\text{B5})$$

and the square of the scattering amplitude can be obtained from the t -channel amplitude contained in Eq. (B4) by swapping s and u :

$$\frac{1}{4N_c^2} \sum_{s,c} |\mathcal{M}_t|^2 = \frac{64\pi^2 \alpha_s^2}{9} \left[\frac{2(u - m_f^2 - m_{f'}^2)^2 + t^2 + 2ut}{(t - m_g^2)^2} \right] . \quad (\text{B6})$$

In the case of equal incoming flavors, we have to distinguish two possibilities: (i) the incoming and outgoing pair have equal flavor, and (ii) the incoming and outgoing pair have different flavor. Whereas the second process proceeds via an s -channel only, the first one also has a t -channel available. We now switch our notation to denote the flavor of the incoming pair by f and the flavor of the outgoing pair by f' . The differential cross section then takes the form

$$\frac{d\sigma}{dt} = \frac{1}{16\pi s(s - 4m_f)^2} \frac{1}{4N_c^2} \sum_{s,c} |\mathcal{M}_s - \delta_{f,f'} \mathcal{M}_t|^2 . \quad (\text{B7})$$

The squared transition amplitude can be obtained from Eq. (B4) by making the substitution $s \rightarrow u \rightarrow t \rightarrow s$, i.e. one has

$$\begin{aligned} \frac{1}{4N_c^2} \sum_{s,c} |\mathcal{M}_s - \delta_{f,f'} \mathcal{M}_t|^2 &= \frac{64\pi^2 \alpha_s^2}{9} \left[\frac{2(u - m_f^2 - m_{f'}^2)^2 + s^2 + 2su}{(s - m_g^2)^2} \right. \\ &\quad + \delta_{f,f'} \frac{2(u - 2m_f^2)^2 + t^2 + 2tu}{(t - m_g^2)^2} \\ &\quad \left. - \frac{2}{3} \delta_{f,f'} \frac{(u - 4m_f^2)^2 - 4m_f^4}{(s - m_g^2)(t - m_g^2)} \right] . \end{aligned} \quad (\text{B8})$$

In the massless limit, Eqs. (B4), (B6) and (B8) reduce to the result of Ref. [37].

REFERENCES

- [1] U. Heinz, Phys. Rev. Lett. 51 (1983) 351; Ann. Phys. (NY) 161 (1985) 48.
- [2] H. Th. Elze, M. Gyulassy and D. Vasak, Nucl. Phys. B 276 (1986) 706; Phys. Lett. B 177 (1986) 402.
- [3] U. Vogl and W. Weise, Prog. Part. Nucl. Phys. 27 (1991) 195.
- [4] S. P. Klevansky, Rev. Mod. Phys. 64 (1992) 649.
- [5] T. Hatsuda and T. Kunihiro, Phys. Rep. 247 (1994) 221.
- [6] J. Hüfner, S. P. Klevansky and P. Rehberg, University of Heidelberg Report No. HD-TVP-96-03 (1996), to appear in Physics Reports.
- [7] E. Quack and S. P. Klevansky, Phys. Rev. C 49 (1994) 3283; J. Müller and S. P. Klevansky, Phys. Rev. C 50 (1994) 410; V. Dmitrašinović, H. J. Schulze, R. Tegen and R. H. Lemmer, Ann. Phys. (NY) 238 (1995) 332.
- [8] P. Rehberg, S. P. Klevansky and J. Hüfner, Phys. Rev. C 53 (1996) 410.
- [9] P. Zhuang, J. Hüfner, S. P. Klevansky and L. Neise, Phys. Rev. D 51 (1995) 3728.
- [10] G. Baym, H. Monien, C. J. Pethick and D. G. Ravenhall, Phys. Rev. Lett. 64 (1990) 1867.
- [11] A. Hosoya and K. Kajantie, Nucl. Phys. B 250 (1985) 666.
- [12] P. Danielewicz and M. Gyulassy, Phys. Rev. D 31 (1985) 53.
- [13] P. Koch, B. Müller and J. Rafelski, Phys. Rep. 142 (1986) 167.
- [14] H. W. Barz, B. L. Friman, J. Knoll and H. Schulz, Nucl. Phys. A 519 (1990) 831.
- [15] J. Bolz, U. Ornik and R. M. Weiner, Phys. Rev. C 46 (1992) 2047.
- [16] E. V. Shuryak, Nucl. Phys. A 566 (1994) 559c.
- [17] P. Rehberg and S. P. Klevansky, University of Heidelberg Report No. HD-TVP-95-13 (1995), [hep-ph/9510221](#).

- [18] E. V. Shuryak, Phys. Rep. 61 (1980) 71.
- [19] E. Quack, P. Zhuang, Y. Kalinovsky, S. P. Klevansky and J. Hüfner, Phys. Lett. B 348 (1995) 1.
- [20] A. E. Dorokhov, M. K. Volkov, J. Hüfner, S. P. Klevansky and P. Rehberg, University of Heidelberg Report No. HD-TVP-95-12 (1995).
- [21] P. Rehberg, Yu. L. Kalinovsky and D. Blaschke, University of Rostock Report No. MPG-VT-UR 81/96, in preparation.
- [22] S. R. de Groot, W. A. van Leeuwen, Ch. G. van Weert, *Relativistic Kinetic Theory* (North Holland, Amsterdam, 1980).
- [23] F. Reif, *Fundamentals of Statistical and Thermal Physics* (McGraw-Hill, New York, 1965)
- [24] M. H. Thoma, Phys. Lett. B 269 (1991) 144.
- [25] J. Rafelski and B. Müller, Phys. Rev. Lett. 48 (1982) 1066.
- [26] T. Matsui, B. Svetitsky and L. D. McLerran, Phys. Rev. D 34 (1986) 783.
- [27] T. Alber et al., Z. Phys. C 64 (1994) 195.
- [28] P. Zhuang, J. Hüfner and S. P. Klevansky, Nucl. Phys. A 576 (1994) 525.
- [29] P. Zhuang, Phys. Rev. C 51 (1995) 2256.
- [30] E. Quack and P. A. Henning, Phys. Rev. Lett. 75 (1995) 2811.
- [31] L. Neise, V. Bunakov and J. Hüfner, University of Heidelberg Report No. HD-TVP-94-3 (1994), unpublished.
- [32] A. Hosoya, M. Sakagami and M. Takao, Ann. Phys. (NY) 154 (1984) 229.
- [33] P. Danielewicz, Ann. Phys. (NY) 152 (1984) 239.
- [34] P. A. Henning, Phys. Rep. 253 (1995) 235.
- [35] W. Zhang and L. Wilets, Phys. Rev. C 45 (1992) 1900.
- [36] W. Florkowski, J. Hüfner, S. P. Klevansky and L. Neise, Ann. Phys. (NY) 245 (1996) 445.

[37] R. Cutler and D. Sievers, Phys. Rev. D 17 (1978) 196.

TABLES

TABLE I. Independent processes for qq scattering.

Process	Exchanged Mesons in t Channel	Exchanged Mesons in u Channel
$uu \rightarrow uu$	$\pi, \eta, \eta', \sigma_\pi, \sigma, \sigma'$	$\pi, \eta, \eta', \sigma_\pi, \sigma, \sigma'$
$ss \rightarrow ss$	$\eta, \eta', \sigma, \sigma'$	$\eta, \eta', \sigma, \sigma'$
$ud \rightarrow ud$	$\pi, \eta, \eta', \sigma_\pi, \sigma, \sigma'$	π, σ_π
$us \rightarrow us$	$\eta, \eta', \sigma, \sigma'$	K, σ_K

TABLE II. Independent processes for $q\bar{q}$ scattering.

Process	Exchanged Mesons in s Channel	Exchanged Mesons in t Channel
$u\bar{d} \rightarrow u\bar{d}$	π, σ_π	$\pi, \eta, \eta', \sigma_\pi, \sigma, \sigma'$
$u\bar{s} \rightarrow u\bar{s}$	K, σ_K	$\eta, \eta', \sigma, \sigma'$
$u\bar{u} \rightarrow u\bar{u}$	$\pi, \eta, \eta', \sigma_\pi, \sigma, \sigma'$	$\pi, \eta, \eta', \sigma_\pi, \sigma, \sigma'$
$u\bar{u} \rightarrow d\bar{d}$	$\pi, \eta, \eta', \sigma_\pi, \sigma, \sigma'$	π, σ_π
$u\bar{u} \rightarrow s\bar{s}$	$\eta, \eta', \sigma, \sigma'$	K, σ_K
$s\bar{s} \rightarrow u\bar{u}$	$\eta, \eta', \sigma, \sigma'$	K, σ_K
$s\bar{s} \rightarrow s\bar{s}$	$\eta, \eta', \sigma, \sigma'$	$\eta, \eta', \sigma, \sigma'$

FIGURES

FIG. 1. Feynman diagrams for elastic qq scattering to lowest order in $1/N_c$.

FIG. 2. Comparison of the cross section for $uu \rightarrow uu$ for three flavors (solid line) with the $SU_f(2)$ result of Ref. [9] (dashed line), at $T = 215$ MeV.

FIG. 3. Total cross section for elastic qq scattering involving only light quarks, as a function of \sqrt{s} , at $T = 215\text{MeV}$ and $T = 250\text{MeV}$.

FIG. 4. Total cross section for elastic qq scattering involving at least one strange quark, as a function of \sqrt{s} , at $T = 215\text{MeV}$ (solid lines) and $T = 250\text{MeV}$ (dashed lines).

FIG. 5. Differential cross section for $ud \rightarrow ud$ at $T = 250\text{MeV}$ and $\sqrt{s} = 1$ GeV within the NJL model (solid line) and perturbative QCD (dashed line).

FIG. 6. Feynman diagrams for elastic $q\bar{q}$ scattering to lowest order in $1/N_c$.

FIG. 7. Comparison of the cross section $u\bar{d} \rightarrow u\bar{d}$ calculated as a function of \sqrt{s} and at $T = 215$ MeV for both $SU_f(3)$ (solid line) and $SU_f(2)$ (dashed line).

FIG. 8. Total cross section for $q\bar{q}$ scattering with only light quarks in the initial state, shown as a function of \sqrt{s} , at $T = 215\text{MeV}$.

FIG. 9. Total cross section for $q\bar{q}$ scattering with only light quarks in the initial state, shown as a function of \sqrt{s} , at $T = 250\text{MeV}$.

FIG. 10. Total cross section for $q\bar{q}$ scattering with at least one strange quark in the initial state, shown as a function of \sqrt{s} , at $T = 215\text{MeV}$.

FIG. 11. Total cross section for $q\bar{q}$ scattering with at least one strange quark in the initial state, shown as a function of \sqrt{s} , at $T = 250\text{MeV}$.

FIG. 12. Differential cross section for $u\bar{s} \rightarrow u\bar{s}$ at $T = 250\text{MeV}$ and $\sqrt{s} = 1\text{ GeV}$ within the NJL model (solid line) and perturbative QCD (dashed line).

FIG. 13. Weight function $P(s, T)$ as a function of s for $m_1 = m_2 = m_u$, $T = 215\text{ MeV}$ (solid line) and $T = 250\text{ MeV}$ (dashed line).

FIG. 14. Energy averaged transition rates, shown as a function of the temperature. The pion Mott temperature is indicated by the dashed vertical line.

FIG. 15. Thermal relaxation times for light (solid line) and strange (dashed line) quarks, shown as a function of the temperature. The pion Mott temperature is indicated by the dashed vertical line.

FIG. 16. Mean free path for light (solid line) and strange (dashed line) quarks, shown as a function of the temperature. The pion Mott temperature is indicated by the dashed vertical line.

FIG. 17. Viscosity coefficient per flavor for light (solid line) and strange (dashed line) quarks, shown as a function of the temperature. The vertical dashed line indicates the pion Mott temperature.

FIG. 18. Chemical relaxation times for strange quarks, shown as a function of the temperature. The vertical dashed line indicates the pion Mott temperature. The relaxation time calculated according to Eq. (4.3) is given by the solid line, and according to Eq. (4.5) by the dashed line. The dot-dashed line gives the relaxation time calculated according to Eq. (4.7) with $m_s = 150\text{ MeV}$, while the dotted line gives the relaxation time calculated according to Eq. (4.7), with strange quark mass from Eq. (2.7).

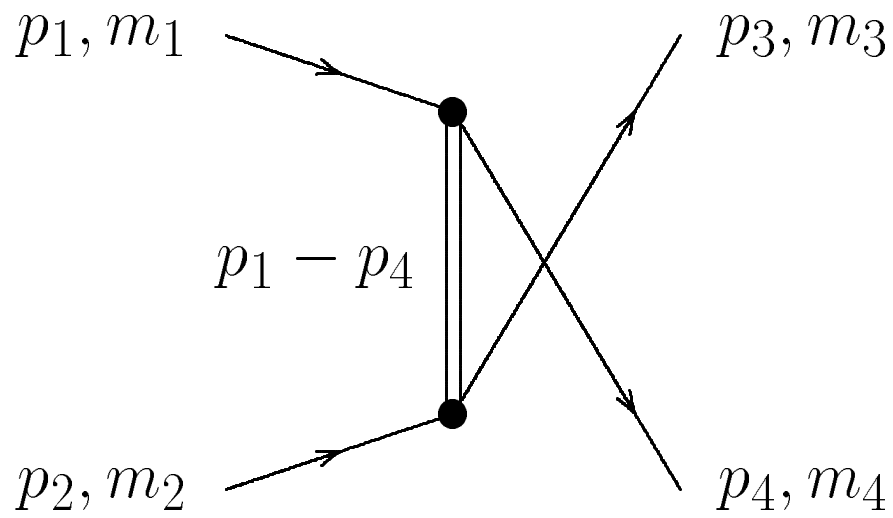
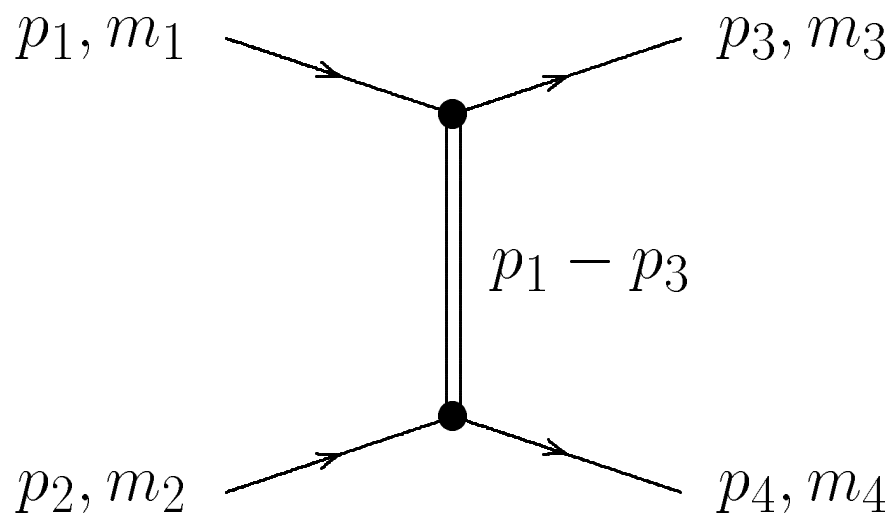


Figure 1

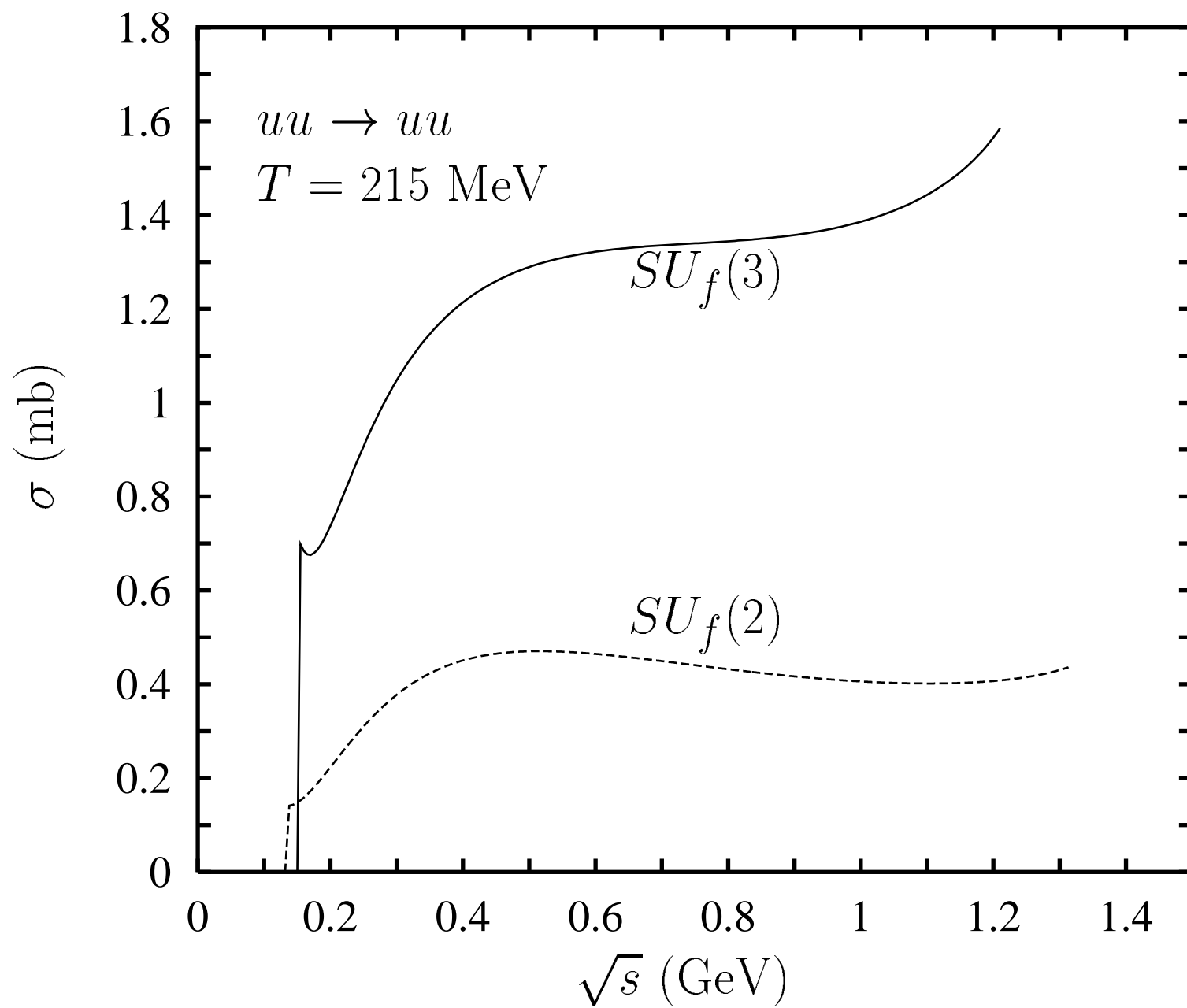
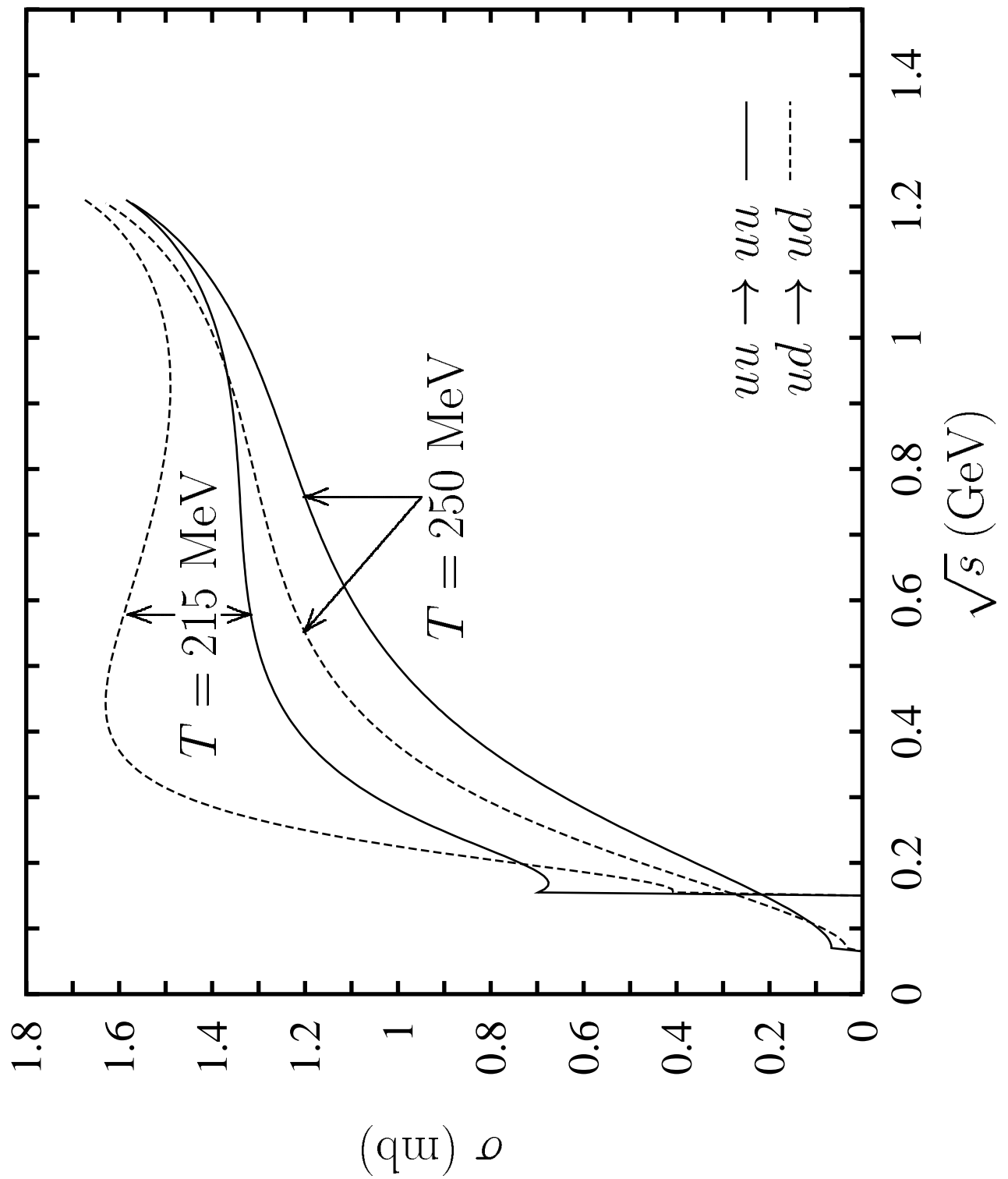


Figure 2

Figure 3



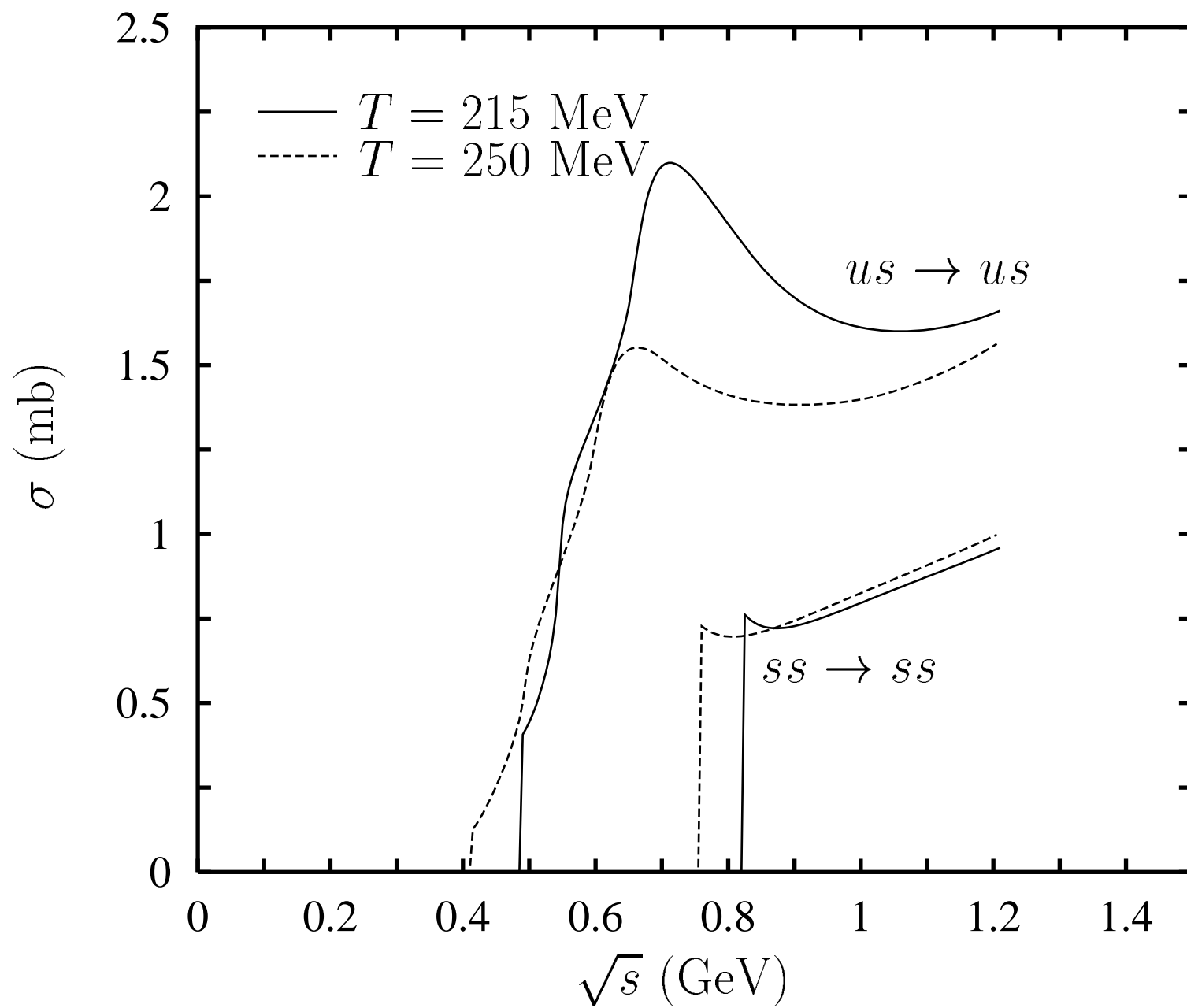


Figure 4

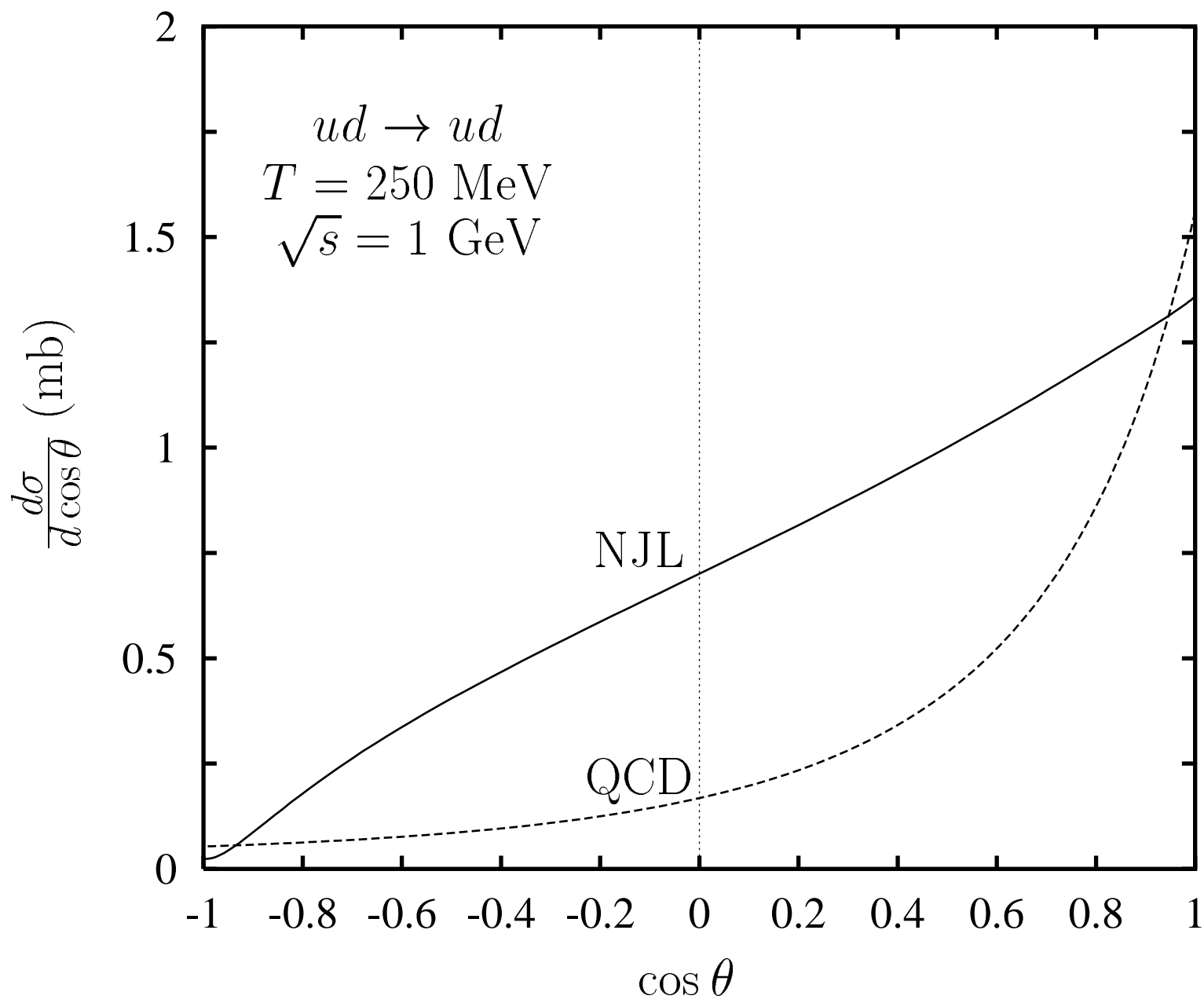


Figure 5

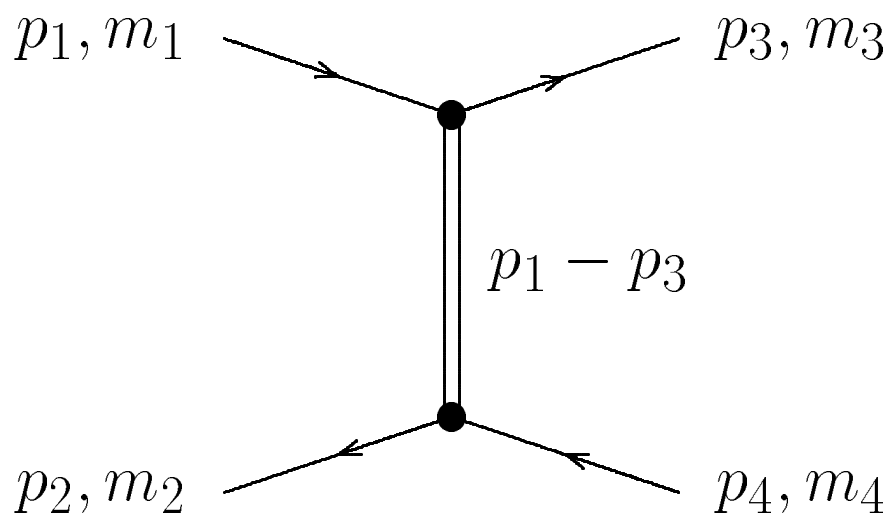
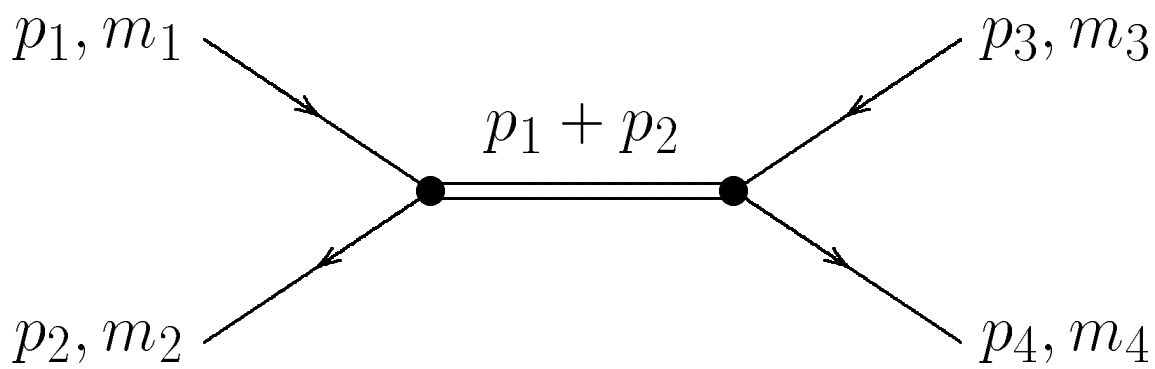
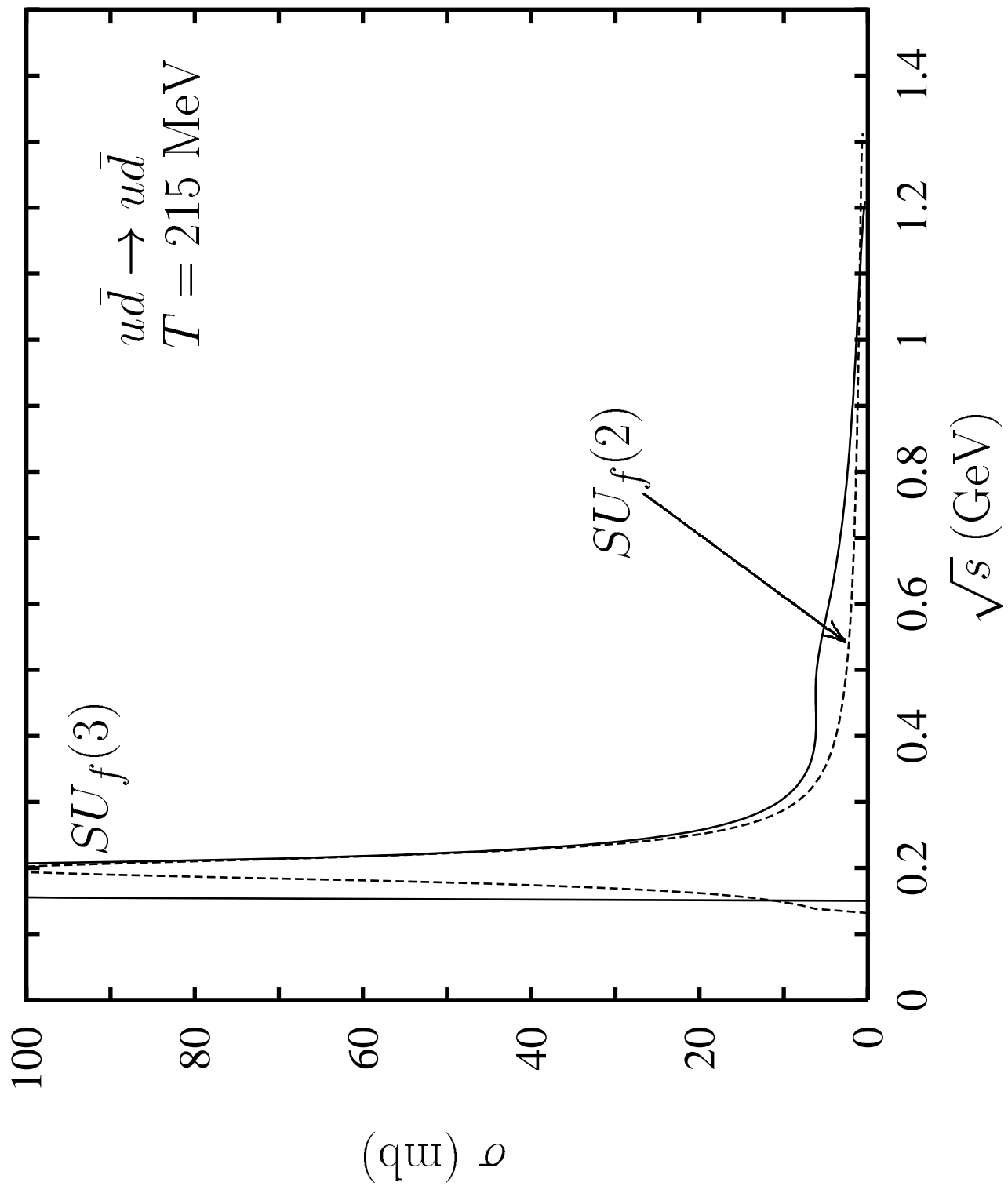


Figure 6

Figure 7



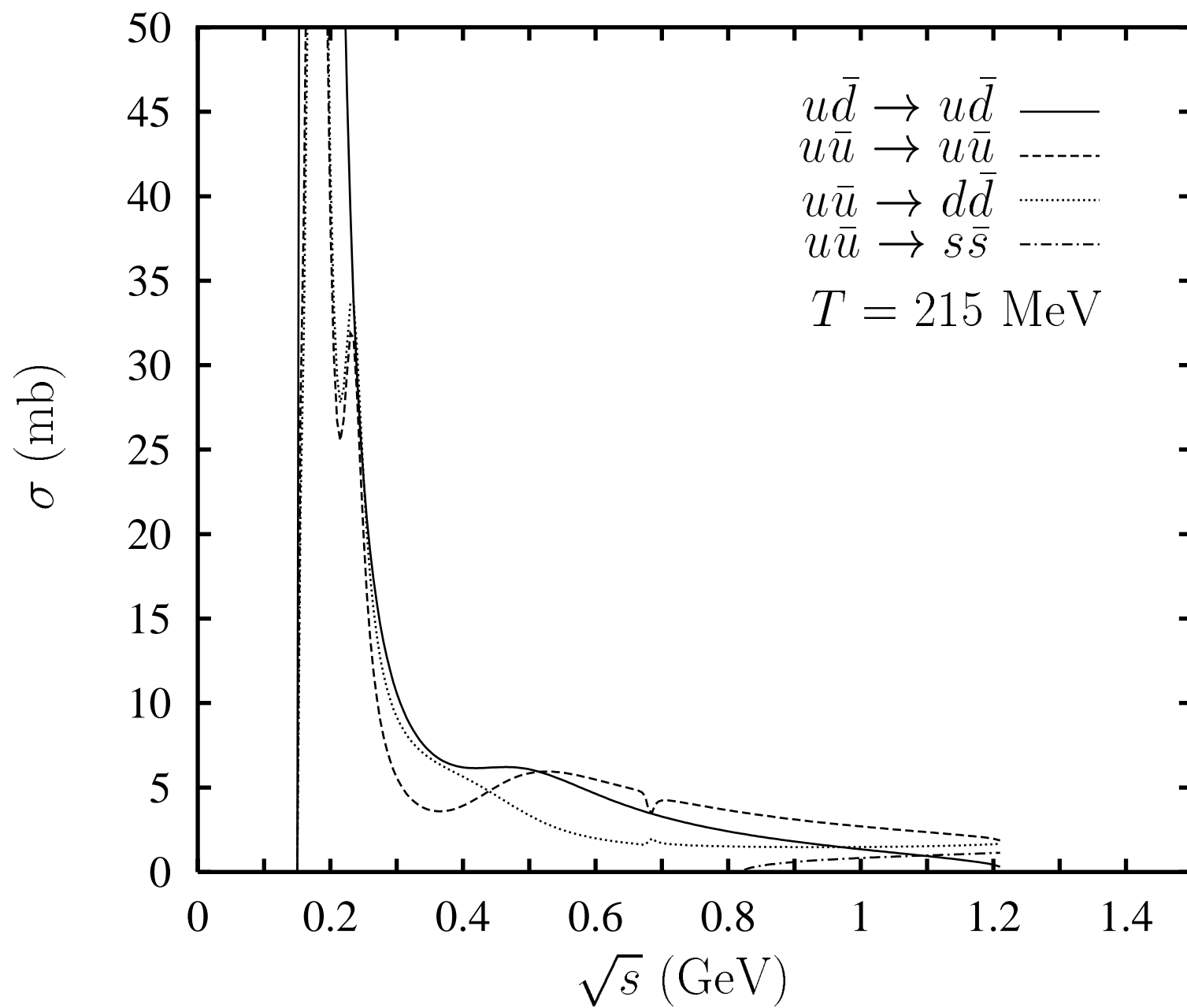


Figure 8

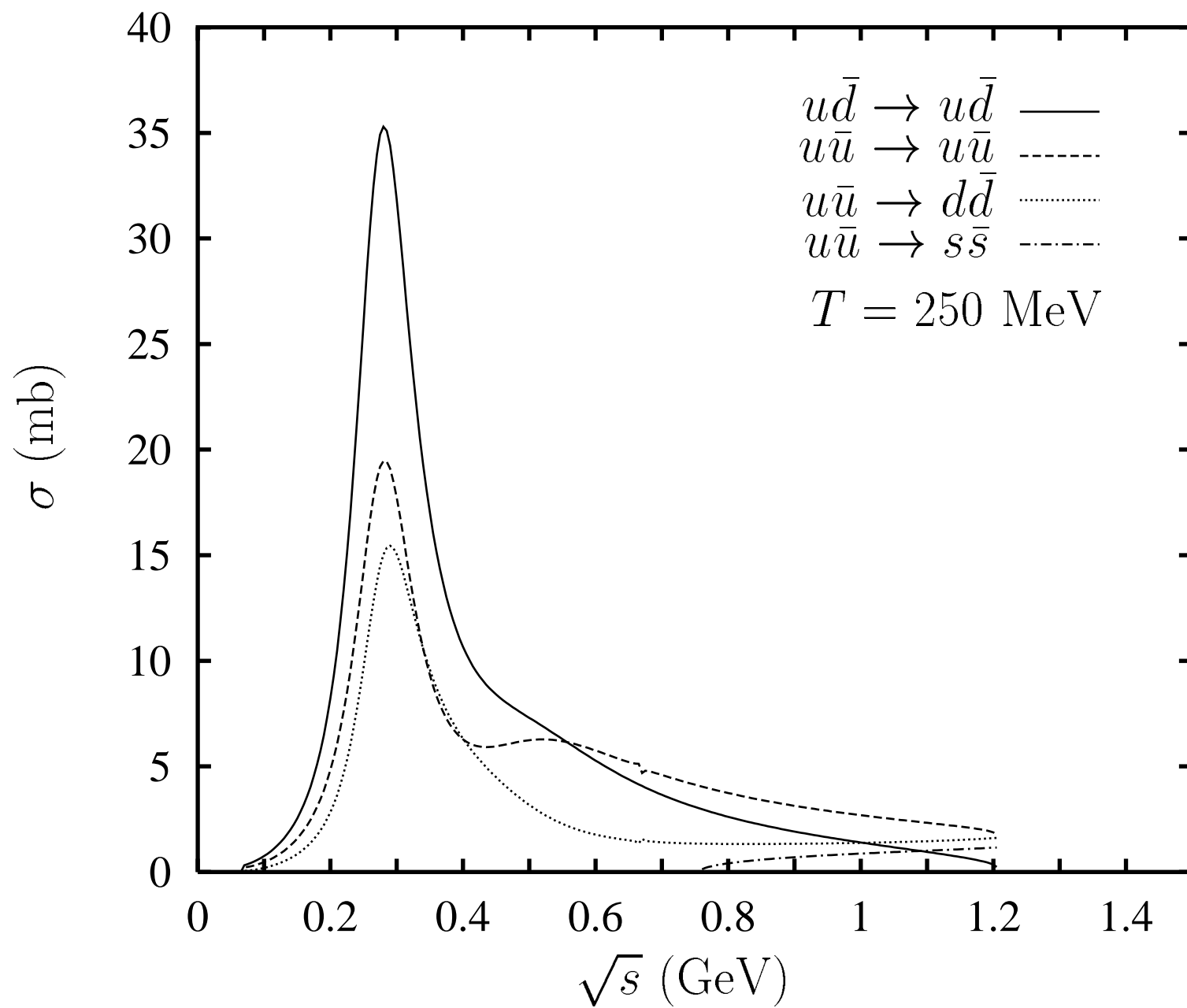


Figure 9

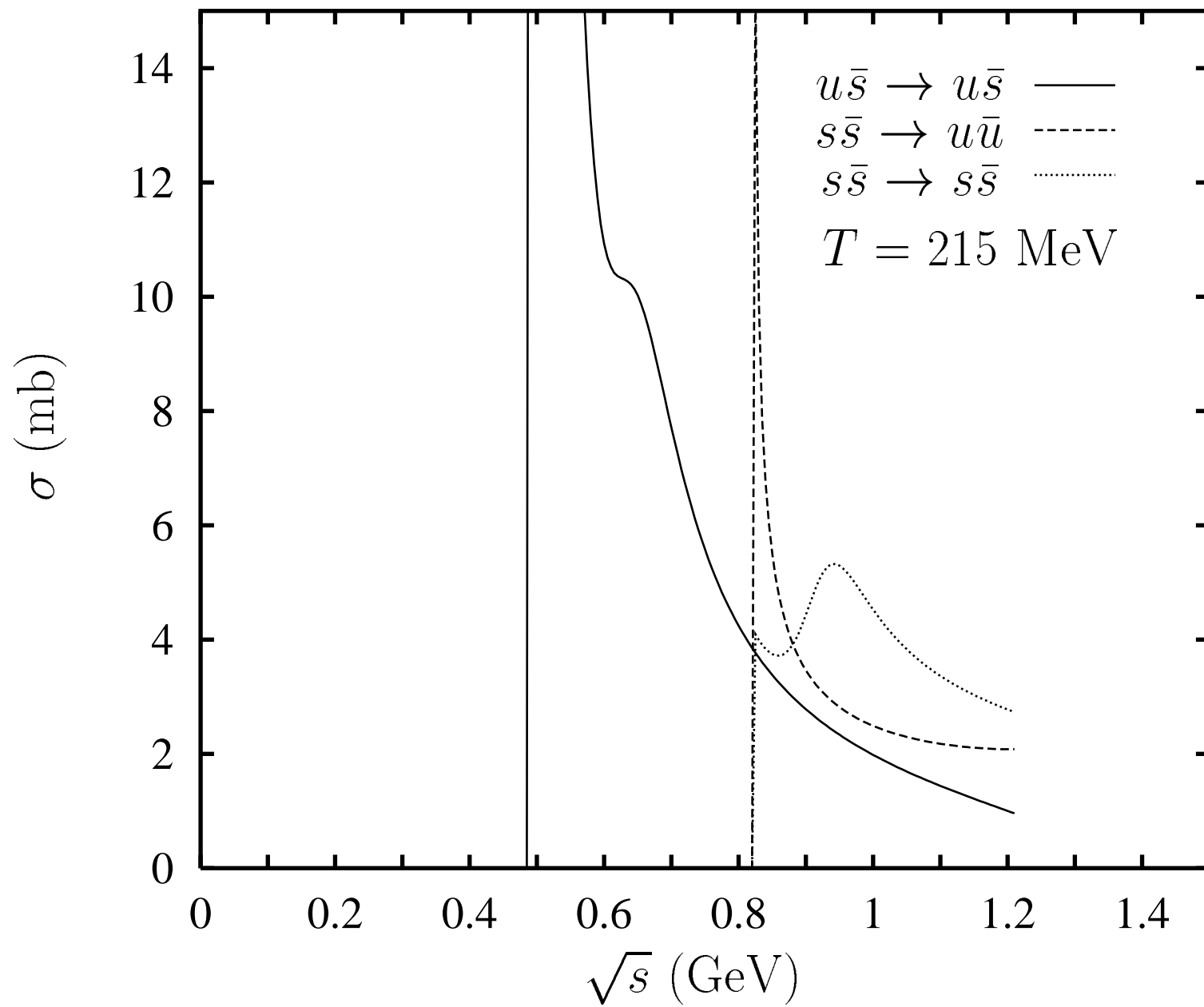


Figure 10

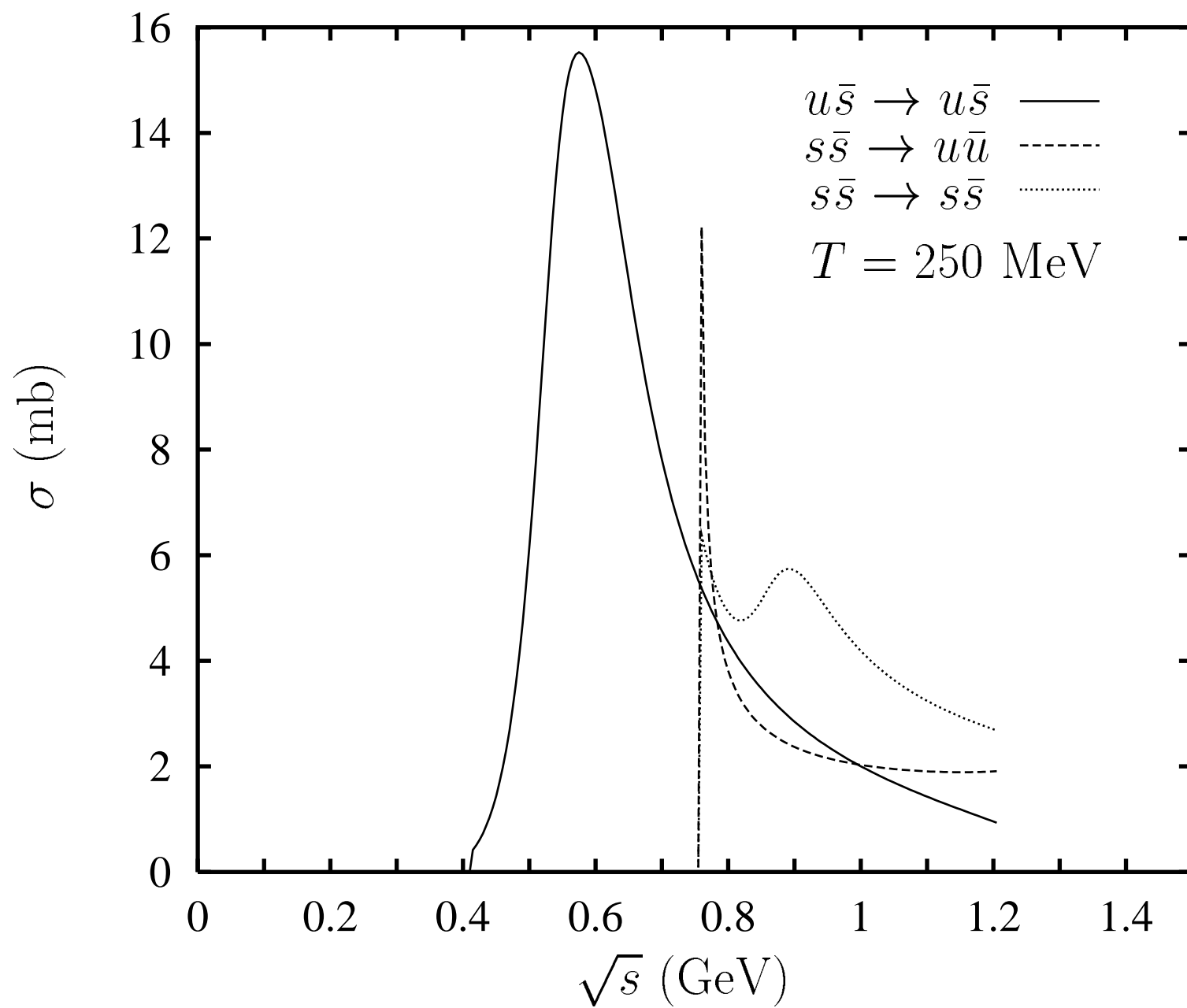


Figure 11

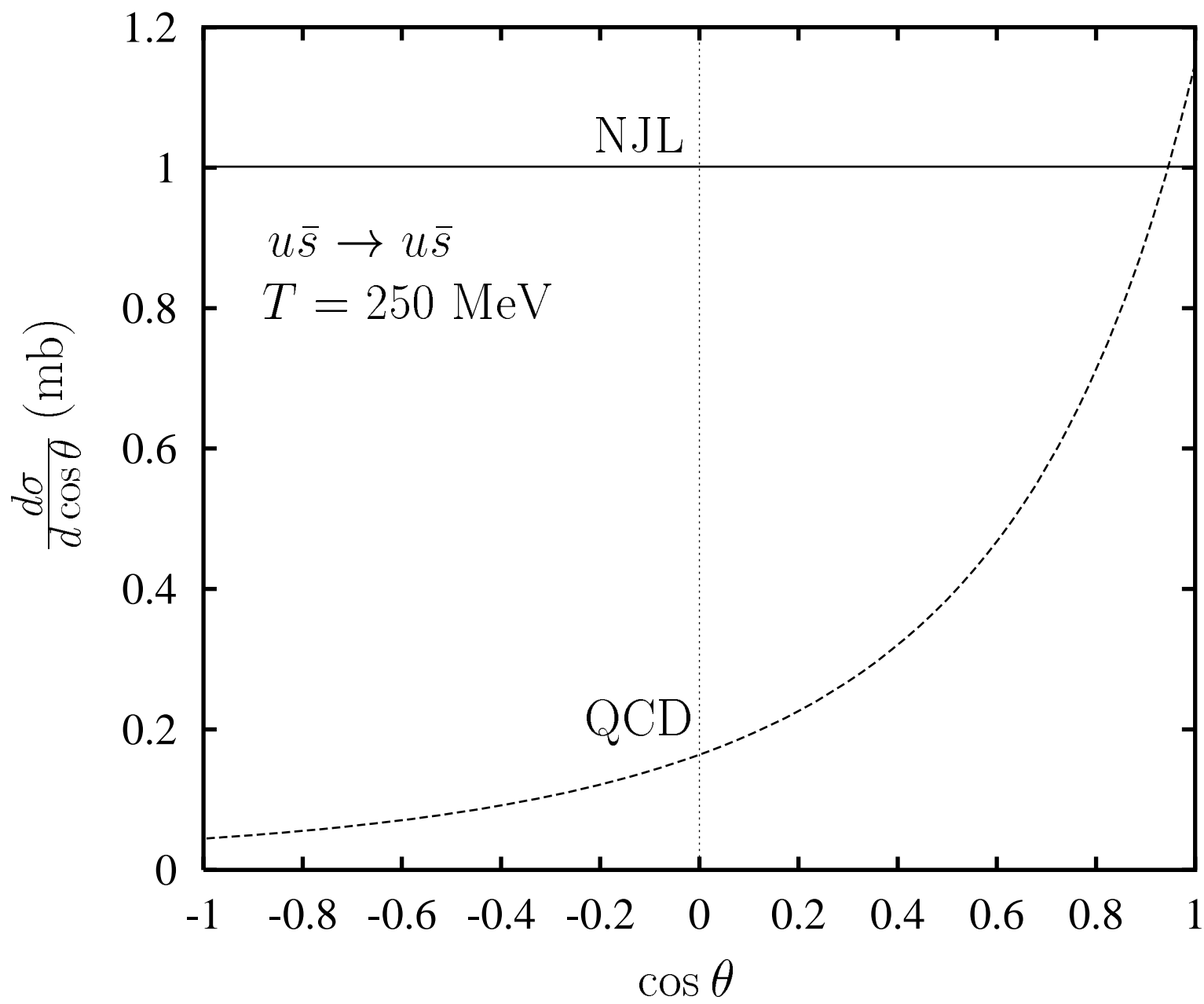


Figure 12

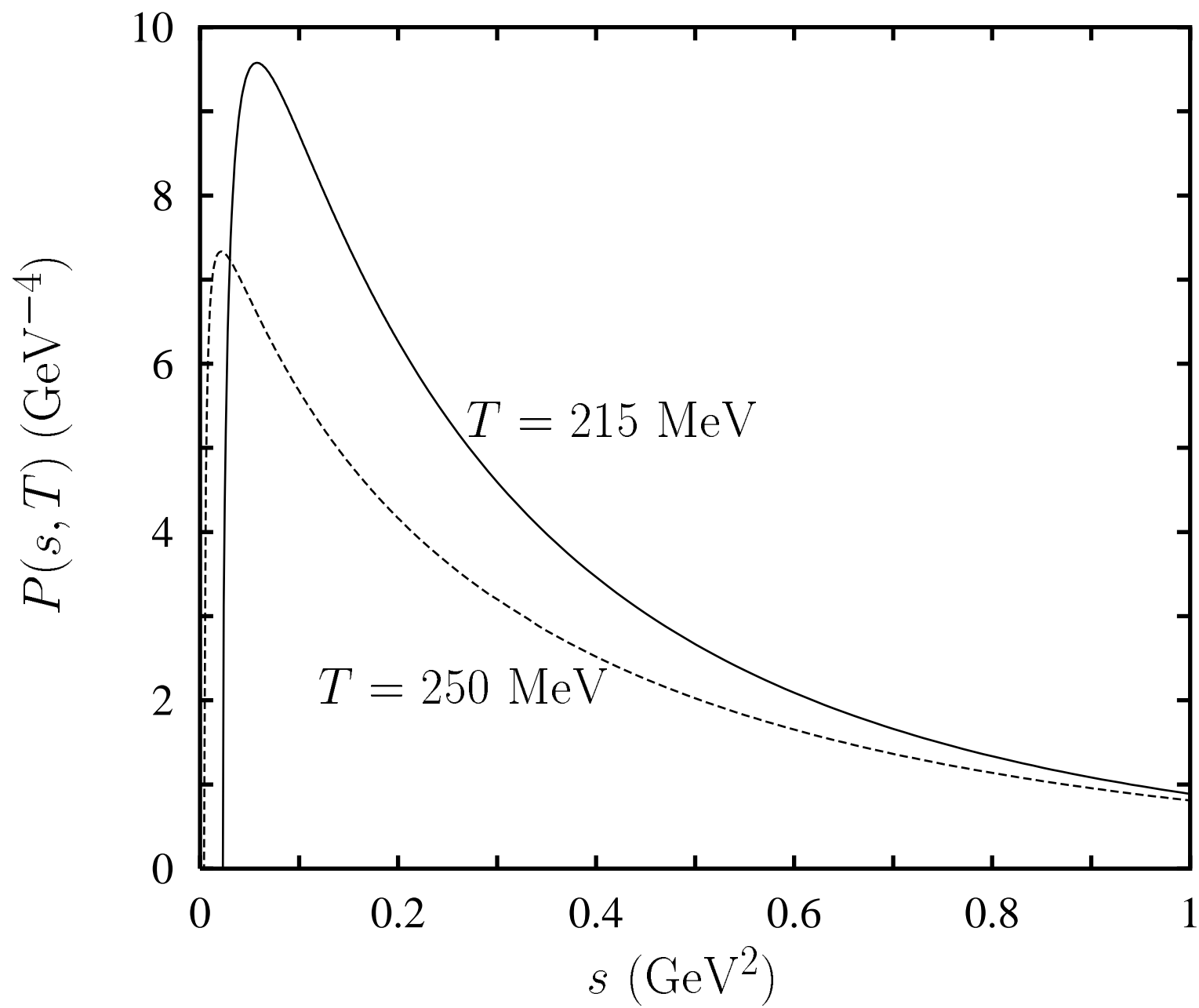


Figure 13

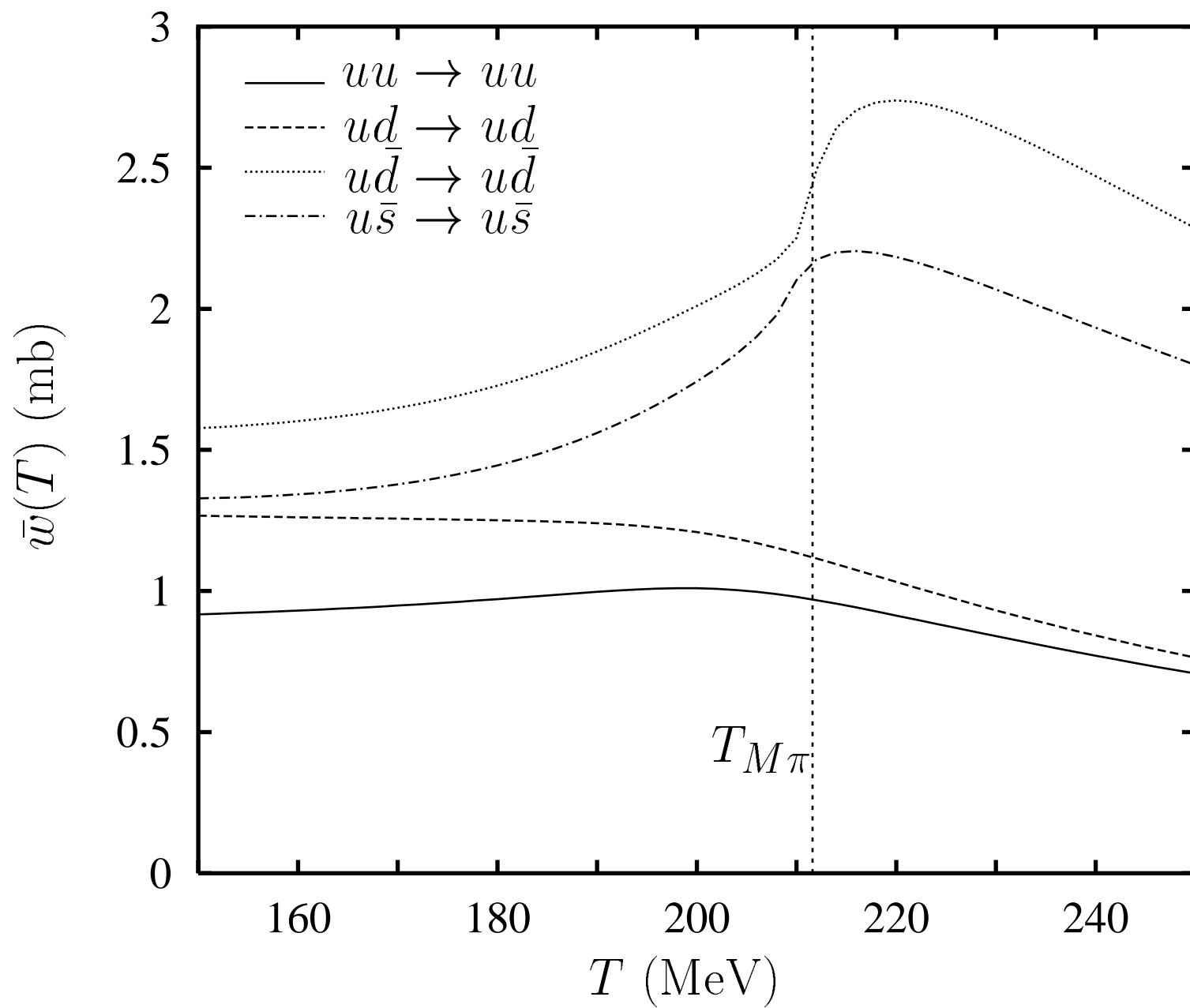


Figure 14

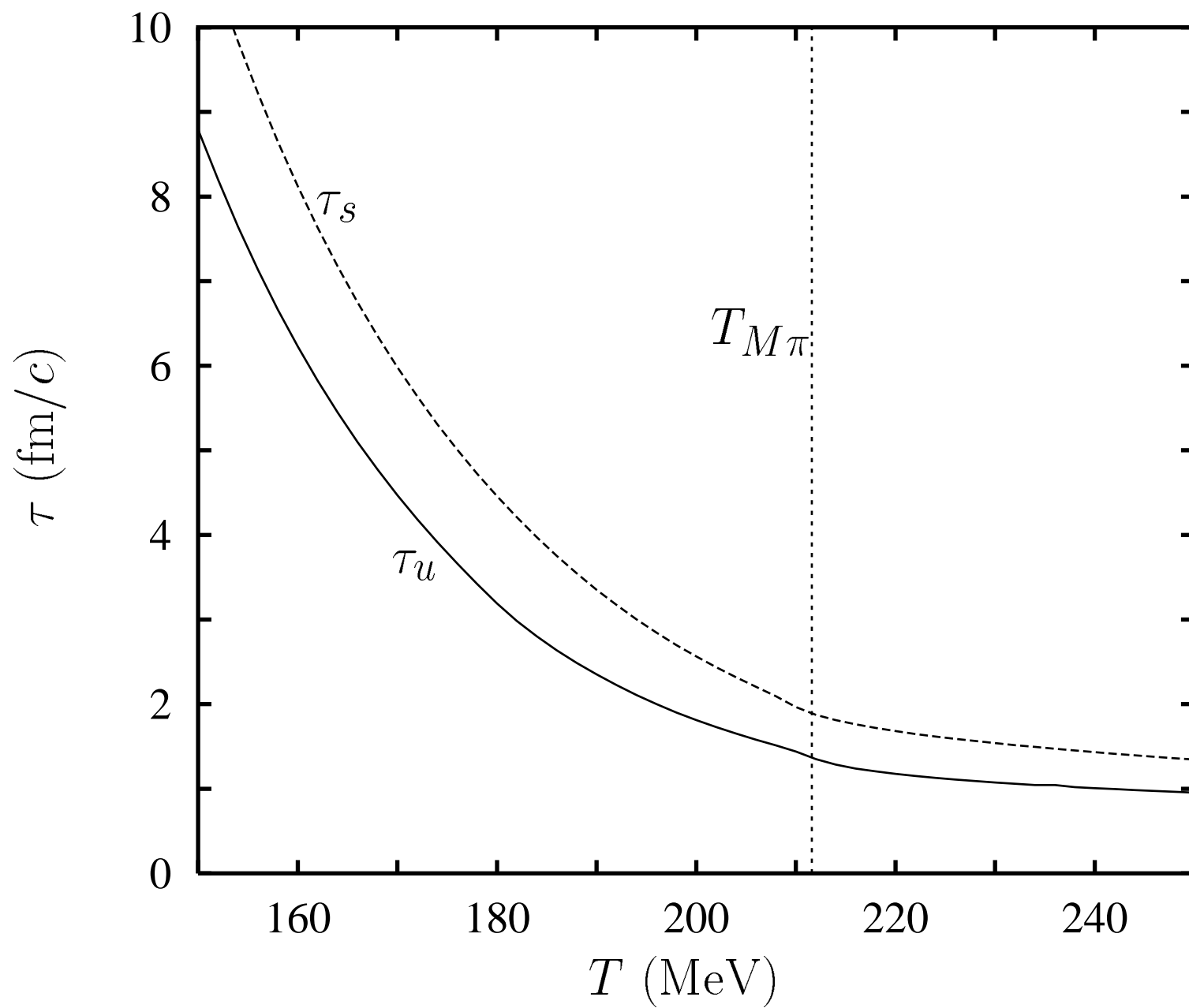


Figure 15

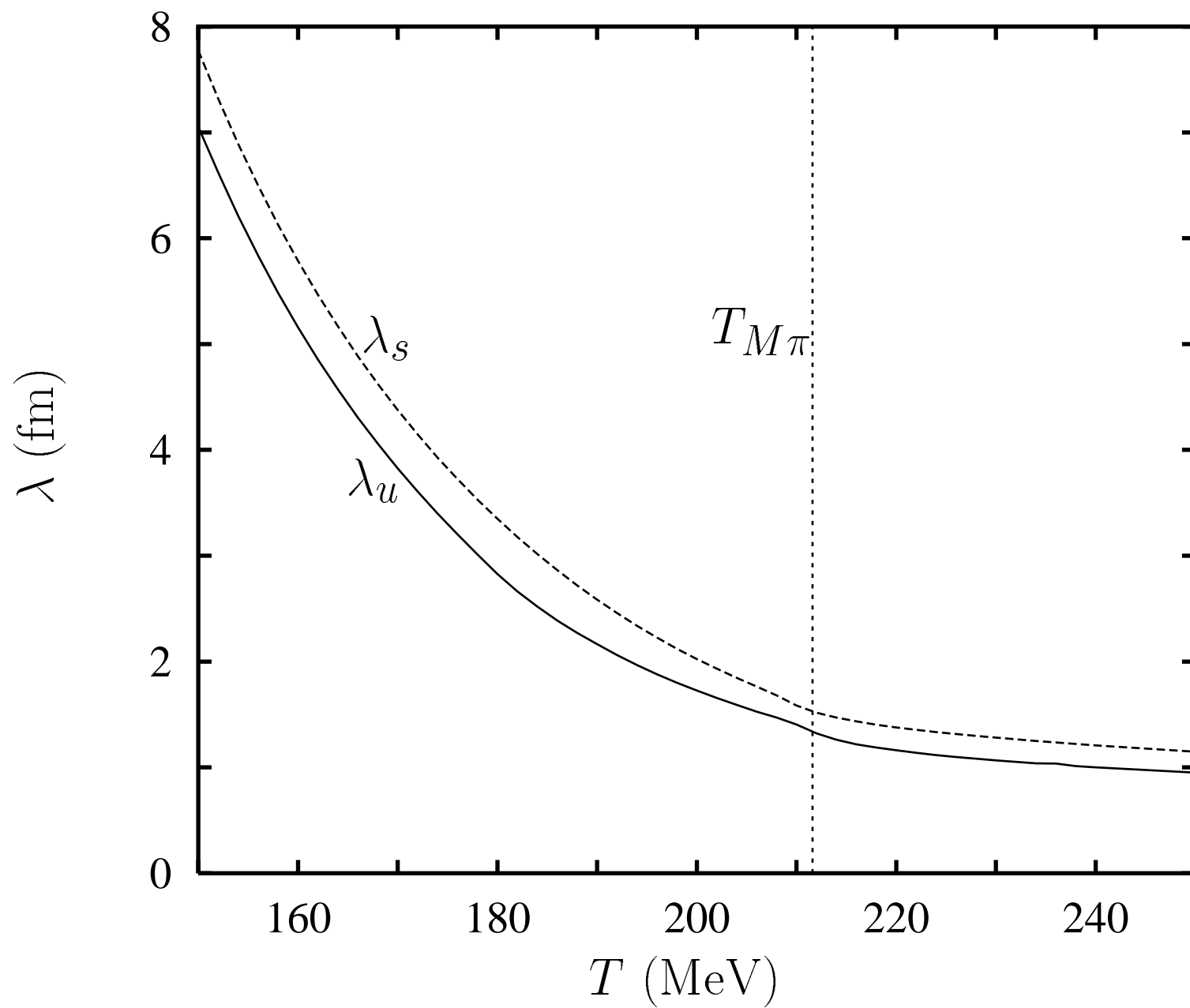


Figure 16

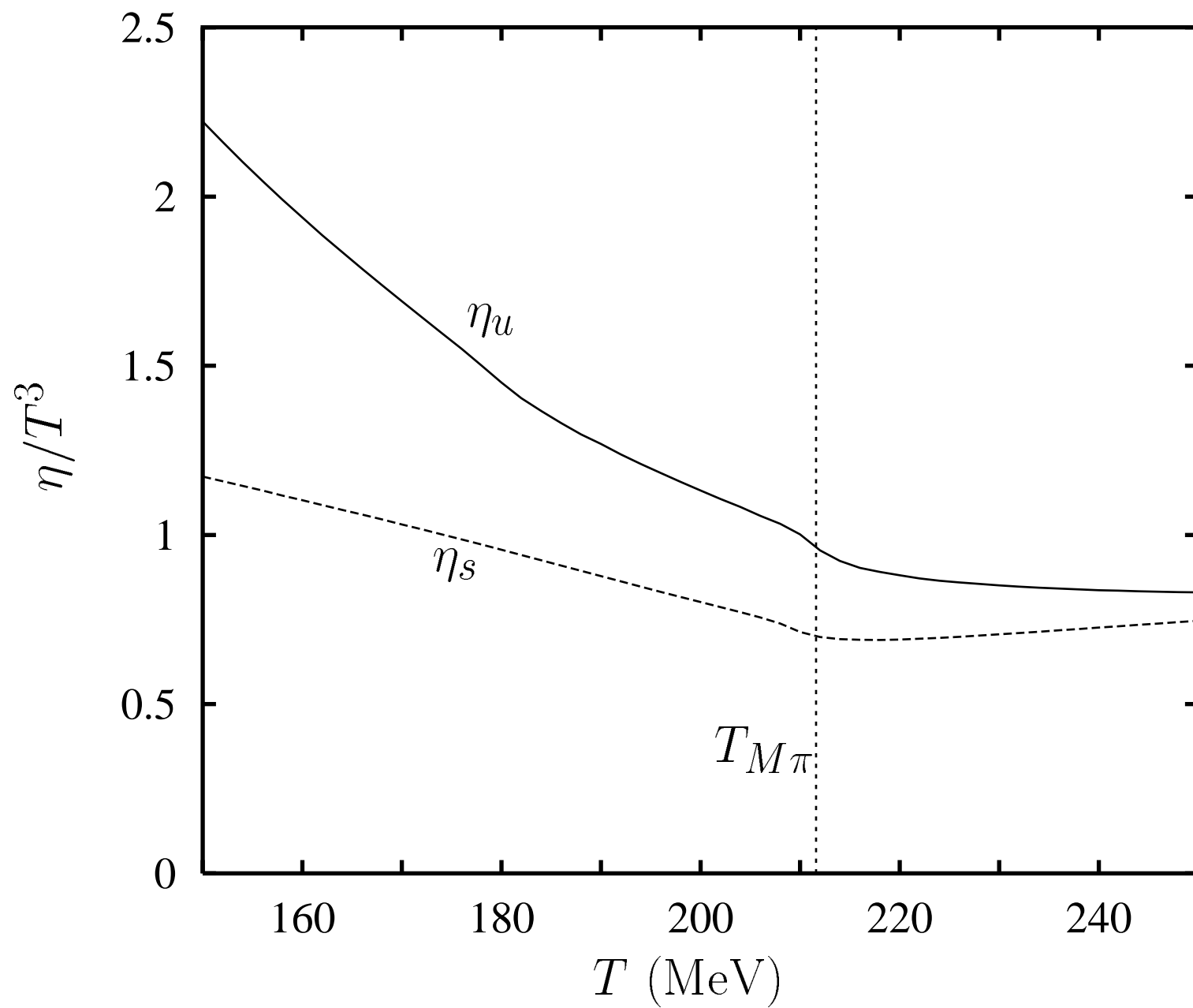


Figure 17

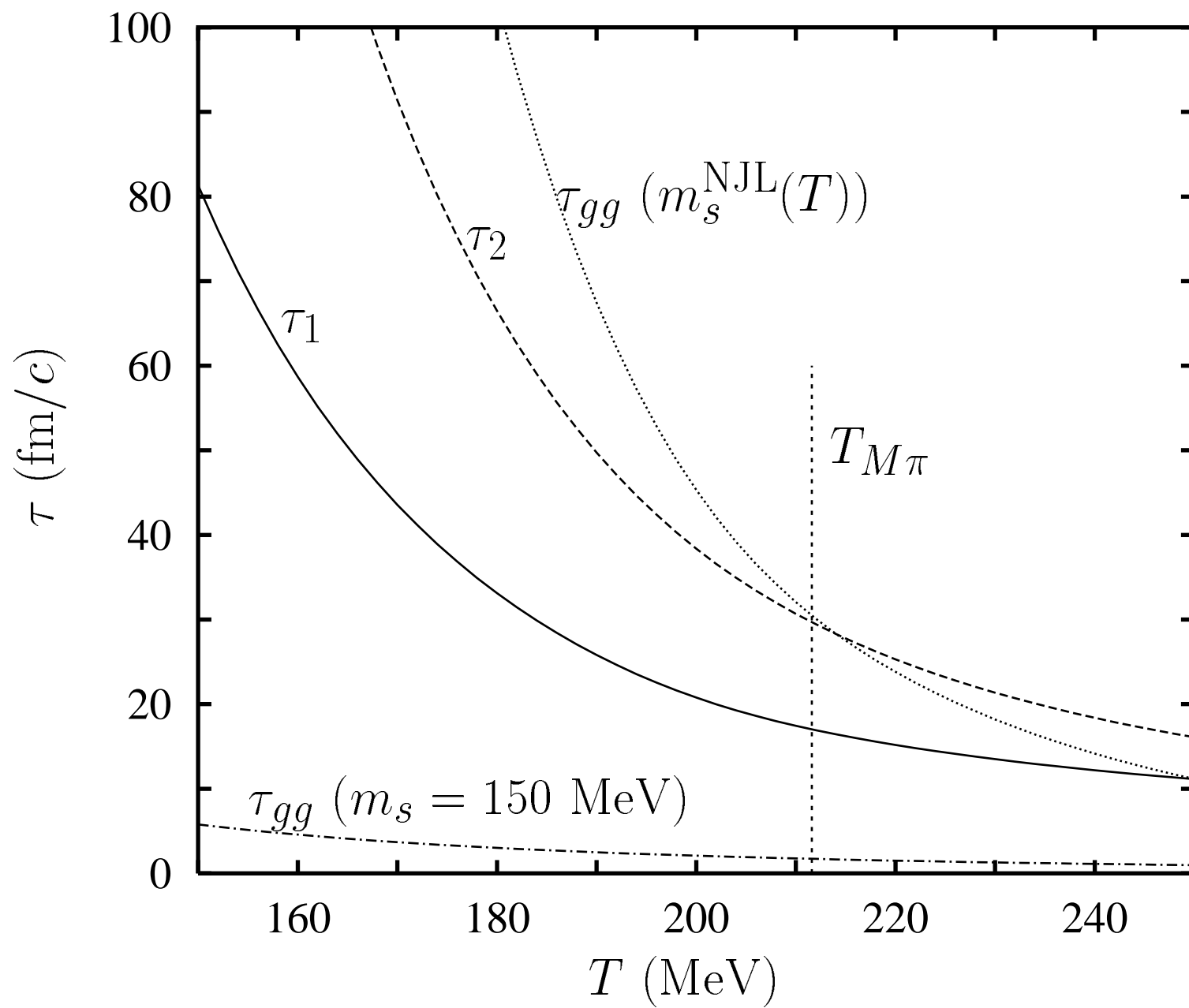


Figure 18